Shift of Macrophage Phenotype Due to Cartilage Oligomeric Matrix Protein Deficiency Drives Atherosclerotic Calcification

Yi Fu,* Cheng Gao,* Ying Liang, Meili Wang, Yaqian Huang, Wei Ma, Tuoyi Li, Yiting Jia, Fang Yu, Wanlin Zhu, Qinghua Cui, Yanhui Li, Qingbo Xu, Xian Wang, Wei Kong

Rationale: **Intimal calcification is highly correlated with atherosclerotic plaque burden, but the underlying mechanism is poorly understood. We recently reported that cartilage oligomeric matrix protein (COMP), a component of vascular extracellular matrix, is an endogenous inhibitor of vascular smooth muscle cell calcification.**

Objective: **To investigate whether COMP affects atherosclerotic calcification.**

Methods and Results: **$ApoE^{-/-}COMP^{-/-}$ mice fed with chow diet for 12 months manifested more extensive atherosclerotic calcification in the innominate arteries than did $ApoE^{-/-}$ mice. To investigate which origins of COMP contributed to atherosclerotic calcification, bone marrow transplantation was performed between $ApoE^{-/-}$ and $ApoE^{-/-}COMP^{-/-}$ mice. Enhanced calcification was observed in mice transplanted with $ApoE^{-/-}COMP^{-/-}$ bone marrow compared with mice transplanted with $ApoE^{-/-}$ bone marrow, indicating that bone marrow–derived COMP may play a critical role in atherosclerotic calcification. Furthermore, microarray profiling of wild-type and $COMP^{-/-}$ macrophages revealed that COMP-deficient macrophages exerted atherogenic and osteogenic characters. Integrin β3 protein was attenuated in $COMP^{-/-}$ macrophages, and overexpression of integrin β3 inhibited the shift of macrophage phenotypes by COMP deficiency. Furthermore, adeno-associated virus 2–integrin β3 infection attenuated atherosclerotic calcification in $ApoE^{-/-}COMP^{-/-}$ mice. Mechanistically, COMP bound directly to β-tail domain of integrin β3 via its C-terminus, and blocking of the COMP–integrin β3 association by β-tail domain mimicked the COMP deficiency–induced shift in macrophage phenotypes. Similar to COMP deficiency in mice, transduction of adeno-associated virus 2–β-tail domain enhanced atherosclerotic calcification in $ApoE^{-/-}$ mice.**

Conclusions: **These results reveal that COMP deficiency acted via integrin β3 to drive macrophages toward the atherogenic and osteogenic phenotype and thereby aggravate atherosclerotic calcification. (*Circ Res*. 2016;119:261-276. DOI: 10.1161/CIRCRESAHA.115.308021.)**

Key Words: atherosclerosis ■ cartilage oligomeric matrix protein ■ extracellular matrix ■ macrophages ■ phenotype ■ vascular calcification

During the past 2 decades, vascular calcification has been increasingly recognized as an independent risk factor for cardiovascular mortality in humans, and there is no pharmacological therapy for this condition.[1–3] The clinical consequences of vascular calcification are largely dependent on its location and extent and on the organs affected. Medial calcification is commonly associated with aging, type II diabetes mellitus, and end-stage renal disease,[4] whereas intimal calcification is highly correlated with atherosclerotic plaque burden.[5] Compelling evidence has indicated that coronary artery calcification is strongly associated with a high risk of cardiovascular events, independently of traditional risk factors. A recent prospective study using ^{18}F-sodium fluoride positron emission tomography further revealed that microcalcification is a good predictor of susceptibility to plaque rupture.[6]

Editorial, see p 184
In This Issue, see p 177

The cellular context of atherosclerotic calcification involves both macrophages and vascular smooth muscle cells (VSMCs).[7] An in vivo genetic fate mapping study revealed that VSMCs in atherosclerotic plaques transdifferentiate into

Original received November 14, 2015; revision received May 3, 2016; accepted May 5, 2015. In April 2016, the average time from submission to first decision for all original research papers submitted to *Circulation Research* was 15.28 days.

From the Department of Physiology and Pathophysiology (Y.F., C.G., Y.L., M.W., Y.H., T.L., Y.J., F.Y., X.W., W.K.), Department of Biomedical Informatics (W.M., Q.C.), Institute of Cardiovascular Sciences, School of Basic Medical Sciences (Y.L.), Peking University, Beijing, P. R. China; Key Laboratory of Molecular Cardiovascular Science, Ministry of Education, Beijing, P. R. China (Y.F., C.G., Y.L., M.W., Y.H., W.M., T.L., Y.J., F.Y., Q.C., Y.L., X.W., W.K.); School of Biological Science and Medical Engineering, International Research Institute for Multidisciplinary Science, Beihang University, Beijing, P. R. China (W.Z.); and Cardiovascular Division, King's College London BHF Centre, London, United Kingdom (Q.X.).

*These authors contributed equally to this article.

The online-only Data Supplement is available with this article at http://circres.ahajournals.org/lookup/suppl/doi:10.1161/CIRCRESAHA.115.308021/-/DC1.

Correspondence to Wei Kong, MD, PhD, Department of Physiology and Pathophysiology, Peking University Health Science Center, 38 Xueyuan Rd, Haidian District, Beijing 100191, P. R. China. E-mail kongw@bjmu.edu.cn

Nonstandard Abbreviations and Acronyms	
AAV	adeno-associated virus
BMDMs	bone marrow–derived macrophages
COMP	cartilage oligomeric matrix protein
IL	interleukin
TLR	toll-like receptor
TNF-α	tumor necrosis factor-α
VSMCs	vascular smooth muscle cells
WT	wild-type

the osteogenic phenotype in a process that mimics osteoblastic differentiation of skeletal bone cells.[8] In contrast, the role of macrophages in lesion calcification is incompletely understood. Although some in vitro coculture studies indicate that monocytes/macrophages enhance VSMC calcification by releasing proinflammatory cytokines,[9–12] other studies proposed that osteogenic VSMCs promote macrophage infiltration into the calcified lesion to form osteoclast-like cells,[13–15] and differentiation of macrophages into osteoclast-like cells may cause the demineralization of elastin-oriented vascular calcification and therefore inhibit the process.[16,17] Further studies using macrophage-specific knockout mice have indicated the importance of the macrophage-derived osteoprotegerin/receptor activator of nuclear factor-κB ligand/receptor activator of nuclear factor-κB triad,[18] glucocorticoid receptor,[19] and matrix vesicles[20] in regulating lesion calcification. Nevertheless, it is still unclear how macrophages affect atherosclerotic calcification and what mediators are involved.

Cartilage oligomeric matrix protein (COMP), a 524-kDa pentameric noncollagenous glycoprotein, is a matricellular protein found in both the musculoskeletal and cardiovascular systems. Our recent studies have shown that COMP plays critical roles in maintaining homeostasis in the cardiovascular system. COMP maintains the contractile phenotype of VSMCs via integrin α7 and prevents osteochondrogenic transdifferentiation of VSMCs by binding directly to bone morphogenetic protein 2, thereby inhibiting VSMCs or medial calcification.[21,22] ADAMTS-7 (a distintegrin and metalloproteinase with thrombospondin motifs), the only COMP-degrading enzyme identified in blood vessels, increases atherosclerotic neointima formation and VSMC calcification.[23,24] Intriguingly, ADAMTS-7 has been shown through genome-wide association studies to be connected with coronary artery heart disease and coronary/aortic calcification in humans.[25–27] Considering the difference between intimal and medial calcification, it is still not clear whether COMP is also involved in atherosclerotic calcification. Here, we show that COMP deficiency switched the macrophage phenotype and contributed directly to atherosclerotic lesion calcification. Mechanistically, COMP regulated the macrophage phenotype via integrin β3.

Methods

Animals

All animal studies followed the guidelines of the Animal Care and Use Committee of Peking University. *COMP*$^{-/-}$ mice in the C57BL/6 background strain were kindly provided by Professor Ake Oldberg from the Department of Cell and Molecular Biology at Lund University, Sweden.[28] *COMP*$^{-/-}$ mice were crossbred with *ApoE*$^{-/-}$ mice in the C57BL/6 background to produce *ApoE*$^{-/-}$*COMP*$^{-/-}$ mice.

Analysis of Atherosclerotic Plaques and Calcification

For morphometric analysis of lesions, cross sections of various artery parts, including aortic root, aortic arch, and innominate artery, were prepared individually. Moving up from the base of heart, aortic root region begins at the first appearance of the valve cups dividing the lumen into 3 distinct regions and ends when the valve cups no longer divide the lumen and the wall seems more rounded and distinct. Aortic arch region for lesion analysis starts at the branch point of innominate artery and then moves backward to the aortic root. Innominate artery region begins at its origin on the outer curve of aortic arch and ends at its first branch, which is divided as right common carotid artery and right subclavian artery. Every 3 continuous 7-μm-thick sections were made on separate slides without interval for aortic root and with 70-μm intervals for aortic arch and innominate artery, respectively, with a cryostat through these arterial parts. For each mouse, 3 sets of 10 interval sections were applied for Oil Red O, von Kossa, and Movat pentachrome stainings. Staining data (in %) for each mouse were presented as the mean of 10 sections.

Real-Time Polymerase Chain Reaction

SYBR Green 2× polymerase chain reaction mix (TransGen Biotech, Beijing, China) was used according to the manufacturer's instructions. Primers used in the present study are listed in Online Table I.

Statistical Analysis

Values are expressed as mean±SEM. Treatment group values were compared with their controls using GraphPad Prism 6.0 (GraphPad Software, San Diego, CA). In all cases, statistical significance was included where the 2-tailed probability was <0.05.

More detailed Methods are available in the Online Data Supplement.

Results

ApoE$^{-/-}$*COMP*$^{-/-}$ Mice Fed With Chow Diet Develop Cartilaginous Metaplasia and Atherosclerotic Calcification

To investigate the role of COMP in atherosclerotic calcification, we first compared lesion formation and development between 12-month-old *ApoE*$^{-/-}$ and *ApoE*$^{-/-}$*COMP*$^{-/-}$ male mice fed with normal chow diet. There were no differences in body weight, blood pressure, blood cell profile, serum lipids, or biochemical indexes between these 2 genotypes (Online Table II). However, aortic en face Oil Red O staining showed that *ApoE*$^{-/-}$*COMP*$^{-/-}$ mice developed more extensive atherosclerotic lesions than *ApoE*$^{-/-}$ mice (Online Figure IA). Furthermore, we analyzed atherosclerotic plaques in the following artery locations: aortic root, aortic arch, and innominate artery. Oil Red O staining showed that plaques in all 3 locations were increased markedly in *ApoE*$^{-/-}$*COMP*$^{-/-}$ mice compared with their *ApoE*$^{-/-}$ littermates (Online Figure IB and IC). In addition, Movat pentachrome staining was applied to compare the plaque composition between *ApoE*$^{-/-}$ and *ApoE*$^{-/-}$*COMP*$^{-/-}$ mice in innominate artery.[29] As shown in Movat staining in Figure 1A, cartilaginous matrices consisting of a collagen- (yellow) and proteoglycan- (blue) rich extracellular matrix embedded with chondrocyte-like cells (red arrow) characterized by a relatively large amount of clear cytoplasm surrounded by a lacunar rim were found in deep intima of *ApoE*$^{-/-}$*COMP*$^{-/-}$ mice but barely in *ApoE*$^{-/-}$ mice (Figure 1B). In accordance, the chondrocyte-like cells within

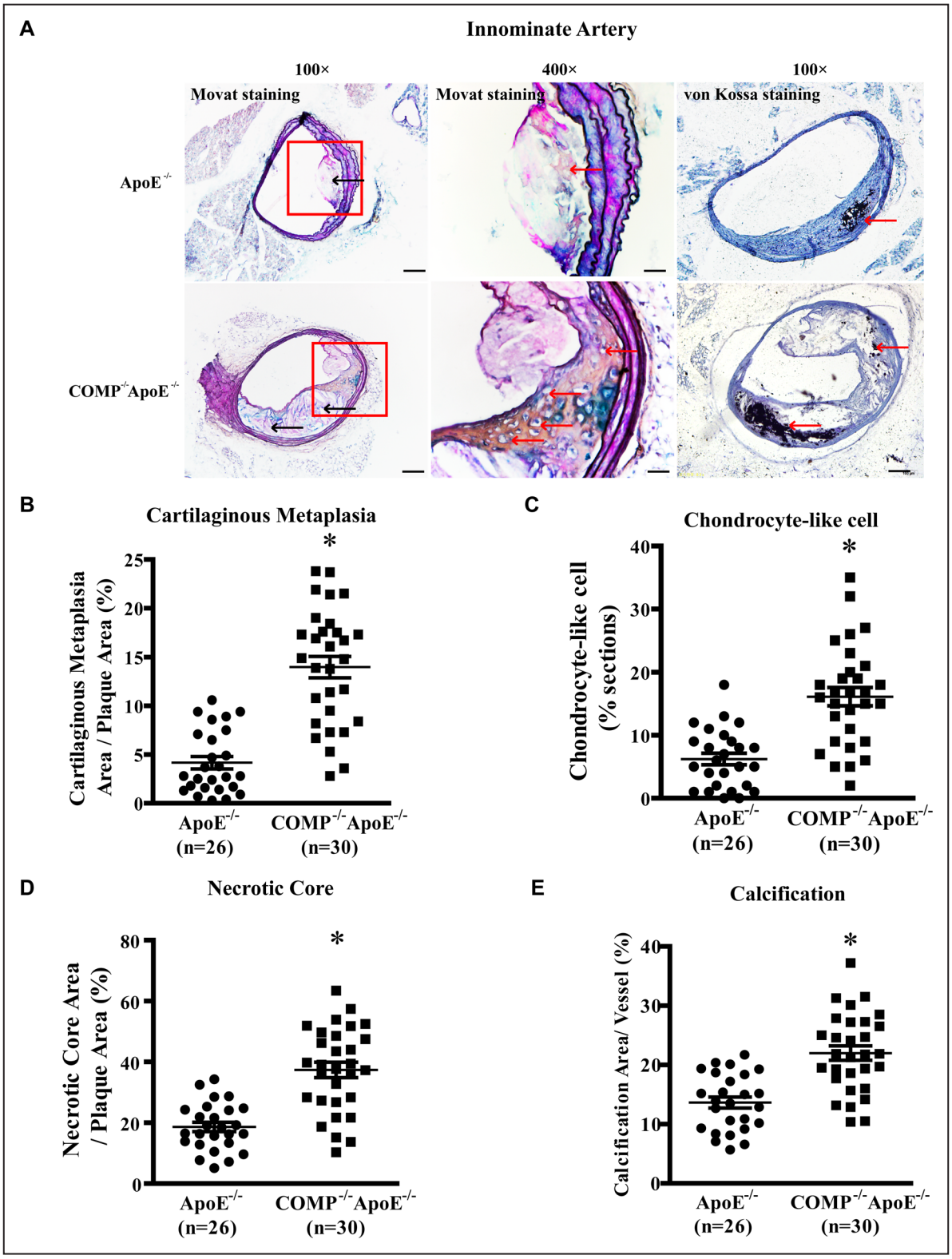

Figure 1. Cartilage oligomeric matrix protein (COMP) deficiency accelerates cartilaginous metaplasia and atherosclerotic calcification. A, Representative images of Movat and von Kossa stainings on cross sections of innominate arteries from 12-month-old *ApoE*$^{-/-}$ and *ApoE*$^{-/-}$*COMP*$^{-/-}$ mice fed with chow diet. Black arrows indicate necrotic core, whereas red arrows indicate chondrocyte-like cells in Movat staining. Scale bar, 100 μm (×100) and 20 μm (×400). Statistical analysis in the percentages of cartilaginous metaplasia area (**B**), plaque-containing chondrocyte-like cells (**C**), and necrotic core area (**D**) in atherosclerotic lesion. **E**, Quantification of calcification areas indicated by red arrow in von Kossa staining. *P<0.05.

lesions implying the early signature of atherosclerotic calcification were markedly increased with COMP deficiency (Figure 1C). The area of necrotic core (black arrow) was significantly elevated in 12-month-old chow-fed *ApoE*$^{-/-}$*COMP*$^{-/-}$ mice (Figure 1D). Further von Kossa staining reinforced greater atherosclerotic calcification in *ApoE*$^{-/-}$*COMP*$^{-/-}$ mice than in *ApoE*$^{-/-}$ mice in all locations, including aortic root, aortic arch, and innominate artery (Figure 1A and 1E; Online Figure II). These results implied that COMP deficiency in *ApoE*$^{-/-}$ mice accelerated the development of atherosclerotic calcification.

Bone Marrow–Derived COMP Is Involved in Atherosclerotic Calcification

Vascular cells and leukocytes are 2 major cellular origins of atherosclerotic lesions and calcification. Therefore, we profiled the expression of COMP and found that COMP expression was high in VSMCs, low in fibroblasts, and undetectable in endothelial cells (Online Figure IIIA). Among unstimulated leukocytes, COMP was mainly detected in macrophages and not in lymphocytes (Online Figure IIIB). To investigate the cell origin of COMP, we isolated bone marrow cells from *ApoE*$^{-/-}$ and *ApoE*$^{-/-}$*COMP*$^{-/-}$ mice and injected them into lethally irradiated male mice of both genotypes, respectively. After bone marrow transplantation, chimeric mice were first genotyped to validate the success of transplantation (Online Figure IV) and then were fed with a Western-type diet for 16 weeks to accelerate the formation of atherosclerotic calcification.[30] There were no differences among the mice fed the Western-type diet in body weight, blood pressure, blood cell profile, serum lipids, and biochemical indexes, including phosphate, calcium, blood urea nitrogen, and creatinine (Online Table III). *ApoE*$^{-/-}$ mice that had received bone marrow from *ApoE*$^{-/-}$*COMP*$^{-/-}$ mice displayed increased plaque formation compared with the recipients of *ApoE*$^{-/-}$ bone marrow (Online Figure VA and VB). *ApoE*$^{-/-}$*COMP*$^{-/-}$ mice transplanted with *ApoE*$^{-/-}$ bone marrow also developed larger atherosclerotic lesions than *ApoE*$^{-/-}$ mice transplanted with *ApoE*$^{-/-}$ bone marrow. This finding indicates that both bone marrow– and non–bone marrow–derived COMPs are involved in atherogenesis. Next, we analyzed lesion compositions of innominate arteries among these chimeric mice. The area of cartilaginous metaplasia and the percentage of chondrocyte-like cells as shown in Movat staining of Figure 2A existed greater in plaques of *ApoE*$^{-/-}$ recipient mice transplanted with *ApoE*$^{-/-}$*COMP*$^{-/-}$ bone marrow compared with *ApoE*$^{-/-}$ chimeric mice. In contrast, no significant difference of the chondrocyte-like cells was observed in atherosclerotic lesions between *ApoE*$^{-/-}$ and *ApoE*$^{-/-}$*COMP*$^{-/-}$ mice receiving *ApoE*$^{-/-}$ bone marrow. Nevertheless, *ApoE*$^{-/-}$*COMP*$^{-/-}$ recipient mice transplanted with *ApoE*$^{-/-}$*COMP*$^{-/-}$ bone marrow showed the most frequent detection of chondrocyte-like cells and the biggest area of cartilaginous metaplasia in plaques compared with other chimeras (Figure 2B and 2C). Similar results were obtained by the use of von Kossa staining to quantify the atherosclerotic calcification in chimeric mice (Figure 2A and 2E). In accordance, the necrotic core area was significantly increased in both genotype mice receiving *ApoE*$^{-/-}$*COMP*$^{-/-}$ bone marrow. Moreover, *ApoE*$^{-/-}$*COMP*$^{-/-}$ mice transplanted with *ApoE*$^{-/-}$ bone marrow also displayed a significant elevation of necrotic core area compared with *ApoE*$^{-/-}$ mice receiving *ApoE*$^{-/-}$ bone marrow, indicating that both bone marrow– and non–bone marrow–derived COMPs contributed to the necrotic core formation in atherosclerosis (Figure 2D). Together, these data suggest that bone marrow cell–derived COMP played a more critical role in atherosclerotic calcification than non–bone marrow–derived COMP. Moreover, there is a synergistic effect on lesion calcification between bone marrow–derived cells and vascular cells.

To further address the cellular origin of COMP in atherosclerotic calcification, we created transgenic mice specifically expressed COMP in VSMCs (*COMP*-Tg) under the control of VSMC promoter SM-22 in the C57/BL6 background (Online Figure VIA). Four independent mouse lines were generated and detected for COMP expression in aorta (Online Figure VIB). We chose the line 3 of mice for subsequent analysis. We further validated that COMP specifically overexpressed in aorta rather than heart, liver, and lung in *COMP*-Tg mice (Online Figure VIC). First, we compared the calcium deposition of high-phosphate-treated aortic rings from wild-type (WT) and SMC *COMP*-Tg mice (Online Figure VID). We found that *COMP*-Tg in VSMCs decreased calcium deposition of aortic rings, indicating that VSMC-derived COMP inhibited VSMC calcification coinciding with our previous data.[22] To further explore the role of VSMC-derived COMP in atherosclerotic calcification, 6-month-old *ApoE*$^{-/-}$ and SMC *COMP*-Tg *ApoE*$^{-/-}$ mice fed with Western-type diet for 12 weeks were applied to evaluate atherosclerotic lesions and calcification. There were no differences in body weight and serum lipids between these 2 genotypes (Online Table IV). Interestingly, *COMP*-Tg in VSMCs attenuated the atherosclerotic plaques but exhibited no effect on the area of cartilaginous metaplasia, the percentage of chondrocyte-like cells, and necrotic core area in *ApoE*$^{-/-}$ mice (Online Figure VIE–VII). These results reinforced that VSMC-derived COMP played a less important role in atherosclerotic calcification than did bone marrow–derived COMP.

COMP Deficiency Primes Macrophages Toward an Atherogenic and Osteogenic Phenotype

To investigate how bone marrow COMP deficiency affects atherosclerotic lesion formation and calcification, we first compared the myeloid differentiation into monocytes and macrophages in WT and *COMP*$^{-/-}$ mice. No significant differences were observed between the 2 mouse genotypes with regard to the numbers of myeloid cells (Gr-1^{+}/CD11b^{+} in bone marrow), circulating ly6C^{low} and ly6C^{high} monocytes (CD11b^{+} ly6C/G^{-} and CD11b^{+}/ly6C^{+} in CD45^{+} blood cells), neutrophils (CD11b^{+}/ly6G^{+} in CD45^{+} blood cells), or peritoneal macrophages (F4/80^{+}/CD11b^{+}), indicating that COMP deficiency might not affect monocyte/macrophage differentiation (Online Figure VIIA–VIIE). Furthermore, we compared the transmigration of circulating mononuclear cells from WT and *COMP*$^{-/-}$ mice through endothelial cell layers (Online Figure VIIF). As a result, the ability of transmigration between WT and *COMP*$^{-/-}$ cells seemed identical, implying that COMP might not affect monocyte transmigration. Next, we characterized the macrophage gene expression profile in the

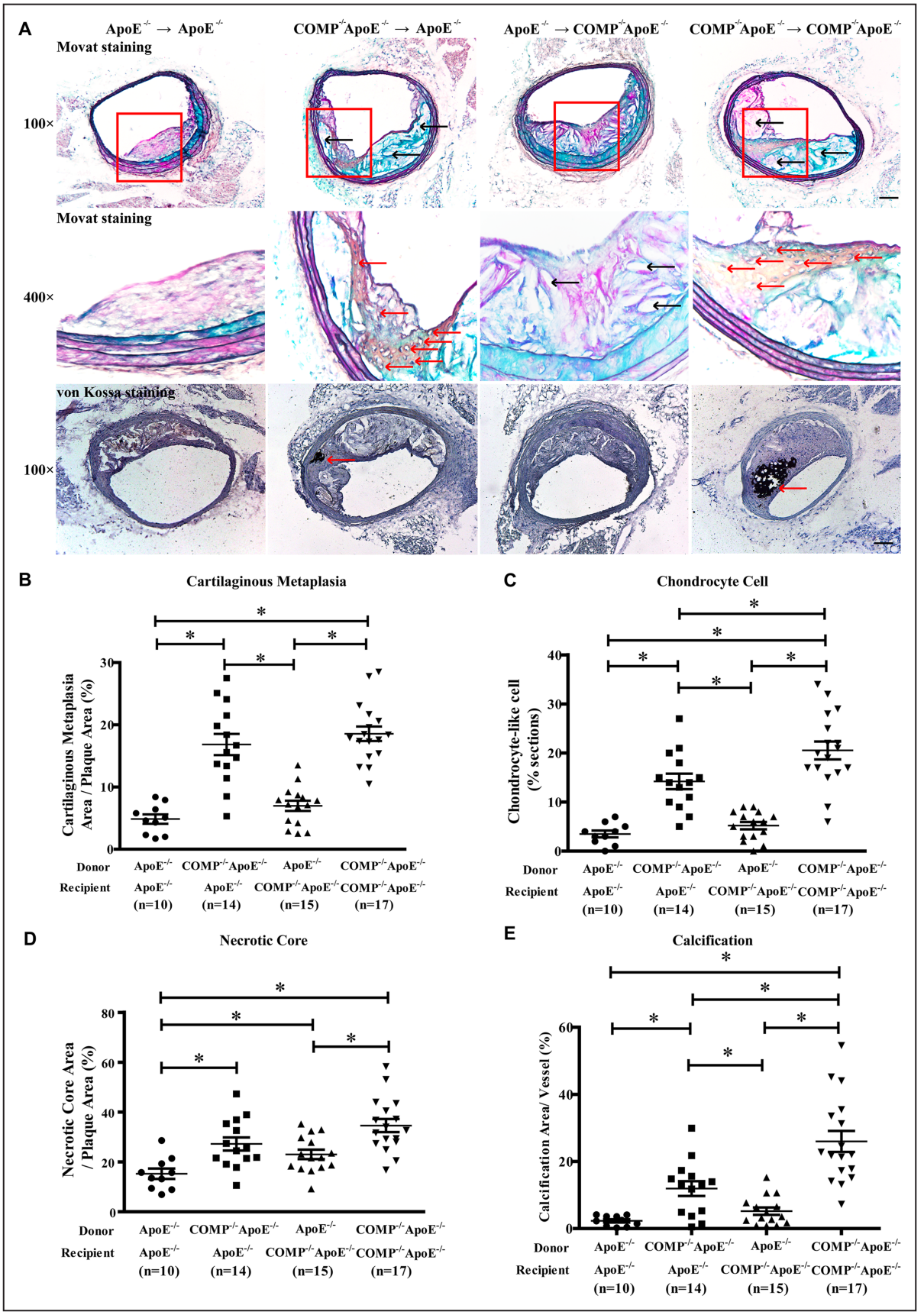

Figure 2. Bone marrow–derived cartilage oligomeric matrix protein (COMP) is involved in cartilaginous metaplasia and atherosclerotic calcification. A, Representative images of Movat and von Kossa stainings on cross sections of innominate arteries from chimeric mice created by bone marrow cross transplantation between *ApoE*$^{-/-}$ and *ApoE*$^{-/-}$*COMP*$^{-/-}$ mice that were fed a Western-type (*Continued*)

Figure 2 Continued. diet for 16 weeks. Black arrows indicate necrotic core, whereas red arrows indicate chondrocyte-like cells in Movat staining. Scale bar, 100 μm (100×) and 20 μm (400×). Statistical analysis in the percentages of cartilaginous metaplasia area (**B**), lesions, including chondrocyte-like cells (**C**), and necrotic core area in atherosclerotic lesion (**D**). **E**, Quantification of calcification areas indicated by red arrow in von Kossa staining. *P<0.05.

absence or presence of COMP. Thioglycollate-elicited peritoneal macrophages from WT and *COMP*$^{-/-}$ mice were profiled for gene expression by microarray. On the basis of array Gene Ontology and Kyoto Encyclopedia of Genes and Genomes analysis, genes involved in multiple pathways, including immune system processes, cell binding, and the toll-like receptor (TLR) signaling pathway, were affected by COMP deficiency (Online Figure VIII). Among the upregulated genes, 4 pathways related to atherosclerosis and calcification were revealed and verified, including inflammation (TLR4, interleukin [IL]-6, tumor necrosis factor-α [TNF-α], and IL-12), reactive oxygen species production (inducible nitric oxide synthase [iNOS] and p47phox), lipid uptake (lectin-type oxidized LDL receptor 1 [LOX-1]), and osteogenesis (Wnt10b and Sphk1; Online Figure IX; Figure 3A–3D). Further bioinformatic correlation analysis of the COMP-deficient macrophage gene profile compared with gene profiles from typical macrophage phenotypes revealed that gene expression by COMP-deficient macrophages positively correlated with gene profiles of the proinflammatory/atherogenic phenotypes (M1 cells activated by interferon-γ/polysaccharide: correlation factor, 0.055 and P=7.95×10^{-13}; M2b cells induced by IL-1β: correlation factor, 0.070 and P<2.2×10^{-16}; Mox cells elicited by oxidative low-density lipoprotein: correlation factor, 0.042 and P=8.907×10^{-08}); however, gene profile of COMP-deficient macrophages negatively correlated with that of the anti-inflammatory (M2c macrophages activated by glucocorticoids: correlation factor, −0.029; P<0.00016) and osteoclast-like phenotypes (correlation factor, −0.029; P=0.00017; Online Table V).

To provide further functional evidence for the macrophage phenotype switch, we measured IL-6 and TNF-α in conditioned medium from peritoneal macrophages; we found that COMP deficiency elevated the secretion of these 2 proinflammatory cytokines (Figure 4A). In addition, the extracellular release of H_2O_2 and the endocytosis of DiI-labeled acetylated low-density lipoprotein were both enhanced in *COMP*$^{-/-}$ peritoneal macrophages compared with WT cells (Figure 4B and 4C). These results indicated that COMP deficiency promoted a proatherosclerotic phenotype in peritoneal macrophages. Next, we tested whether conditioned medium from macrophages lacking COMP would accelerate VSMC calcification (Figure 4D). Indeed, even without high-phosphate treatment, calcium deposition in VSMCs was elevated by conditioned medium from *COMP*$^{-/-}$ macrophages. A further increase in calcium deposition was observed when *COMP*$^{-/-}$ VSMCs were cultured in conditioned medium from *COMP*$^{-/-}$ macrophages, suggesting that VSMCs and macrophages have a

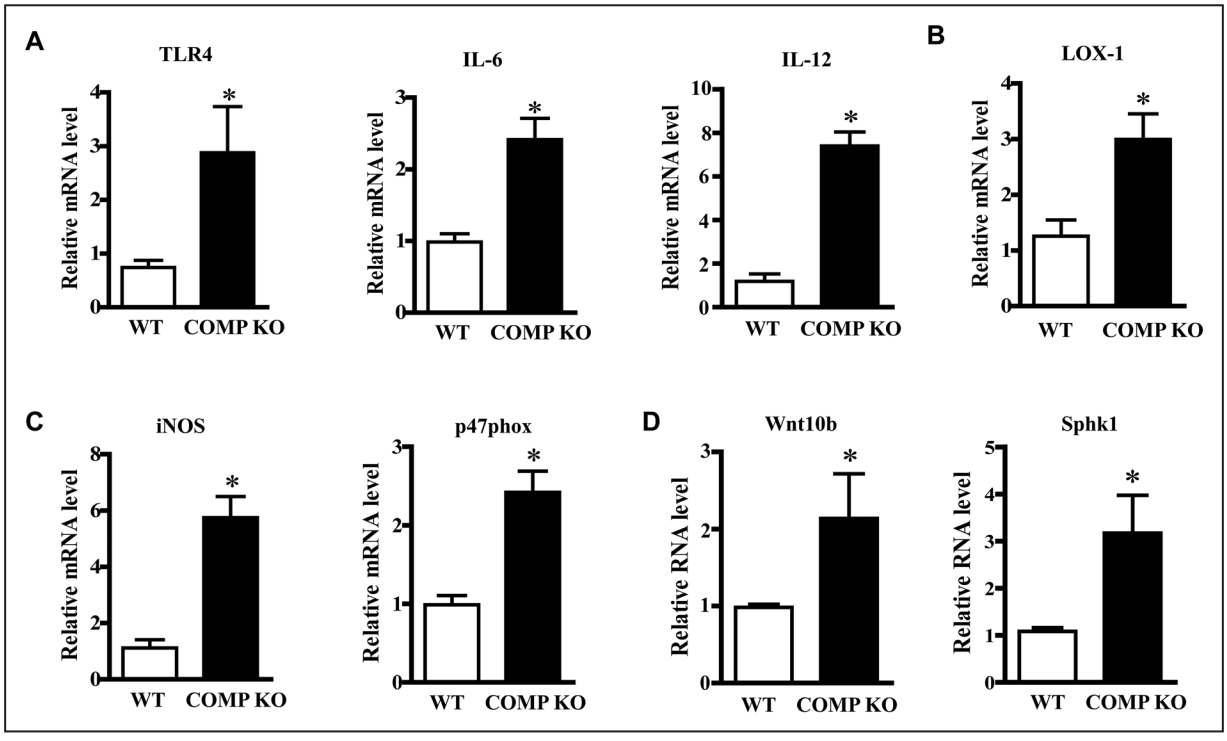

Figure 3. Cartilage oligomeric matrix protein (COMP) deficiency induces profile alteration in gene expression in macrophages. Validation of the upregulated genes associated with inflammation (toll-like receptor 4 [TLR4], interleukin [IL]-6, and IL-12; **A**), endocytosis (LOX-1; **B**), reactive oxygen species production (inducible nitric oxide synthase [iNOS] and p47phox; **C**), and osteogenesis (Wnt10b and Sphk1; **D**) in wild-type (WT) and *COMP*$^{-/-}$ peritoneal macrophages by real-time polymerase chain reaction. n=6; *P<0.05. KO indicates knockout.

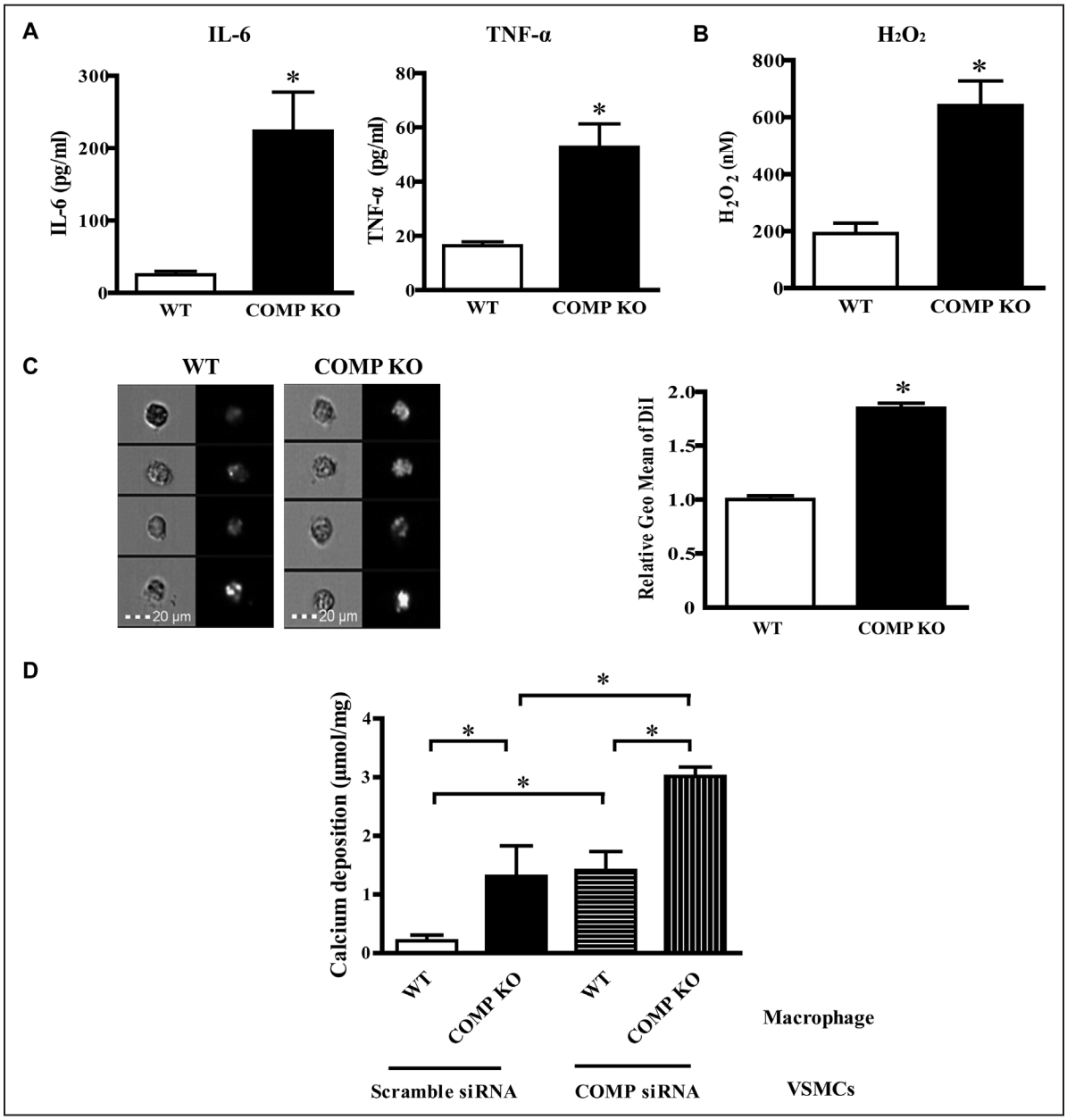

Figure 4. Cartilage oligomeric matrix protein (COMP) deficiency alters the phenotype of macrophages. A, Cytometric bead array measurement of interleukin (IL)-6 and tumor necrosis factor-α (TNF-α) in conditioned medium from wild-type (WT) and *COMP*$^{-/-}$ peritoneal macrophages. **B**, H_2O_2 measurement in conditioned medium from WT and *COMP*$^{-/-}$ peritoneal macrophages. **C**, Representative images of DiI-labeled acetylated low-density lipoprotein endocytosis by WT and *COMP*$^{-/-}$ peritoneal macrophages. Bar graph indicates the quantification of fluorescent intensity taken up by macrophages. The fluorescent intensity of 10 000 cells was collected for each experiment, and 3 independent experiments were performed in duplicate. n=3; **P*<0.05. **D**, A7r5 vascular smooth muscle cells (VSMCs) transfected with control small interfering RNA (siRNA) or COMP siRNA (100 nmol) were cultured with conditioned medium from WT and *COMP*$^{-/-}$ peritoneal macrophages for 12 days, followed by measurement and quantification of calcium deposition. Three independent experiments were performed in duplicate. n=3; **P*<0.05. KO indicates knockout.

synergistic effect on calcification. To verify this observation, we examined bone marrow–derived macrophages (BMDMs) from WT or *COMP*$^{-/-}$ mice. As shown in Online Figure X, interferon-γ–activated BMDMs lacking COMP displayed higher expression levels of IL-12, iNOS, and CD86 than did WT cells (Online Figure XA and XB). Conversely, COMP deficiency decreased the expression of Ym-1, Arg-I (arginase I), and CD206, the anti-inflammatory phenotype markers, in IL-4–induced BMDMs (Online Figure XC and XD). Moreover, increases in H_2O_2 production and Wnt10b gene expression were also observed in COMP-deficient BMDMs (Online Figure XE and XF). Therefore, COMP deficiency may cause macrophage phenotypic switch toward atherogenic and osteogenic phenotype.

COMP$^{-/-}$ Macrophages Exhibit an Atherogenic and Osteogenic Phenotype in Atherosclerotic Lesions

To further evaluate the macrophage phenotypes in atherosclerotic lesions, we used flow cytometry to analyze single-cell suspensions digested from aortic tissue. CD45$^+$ and F4/80$^+$ were

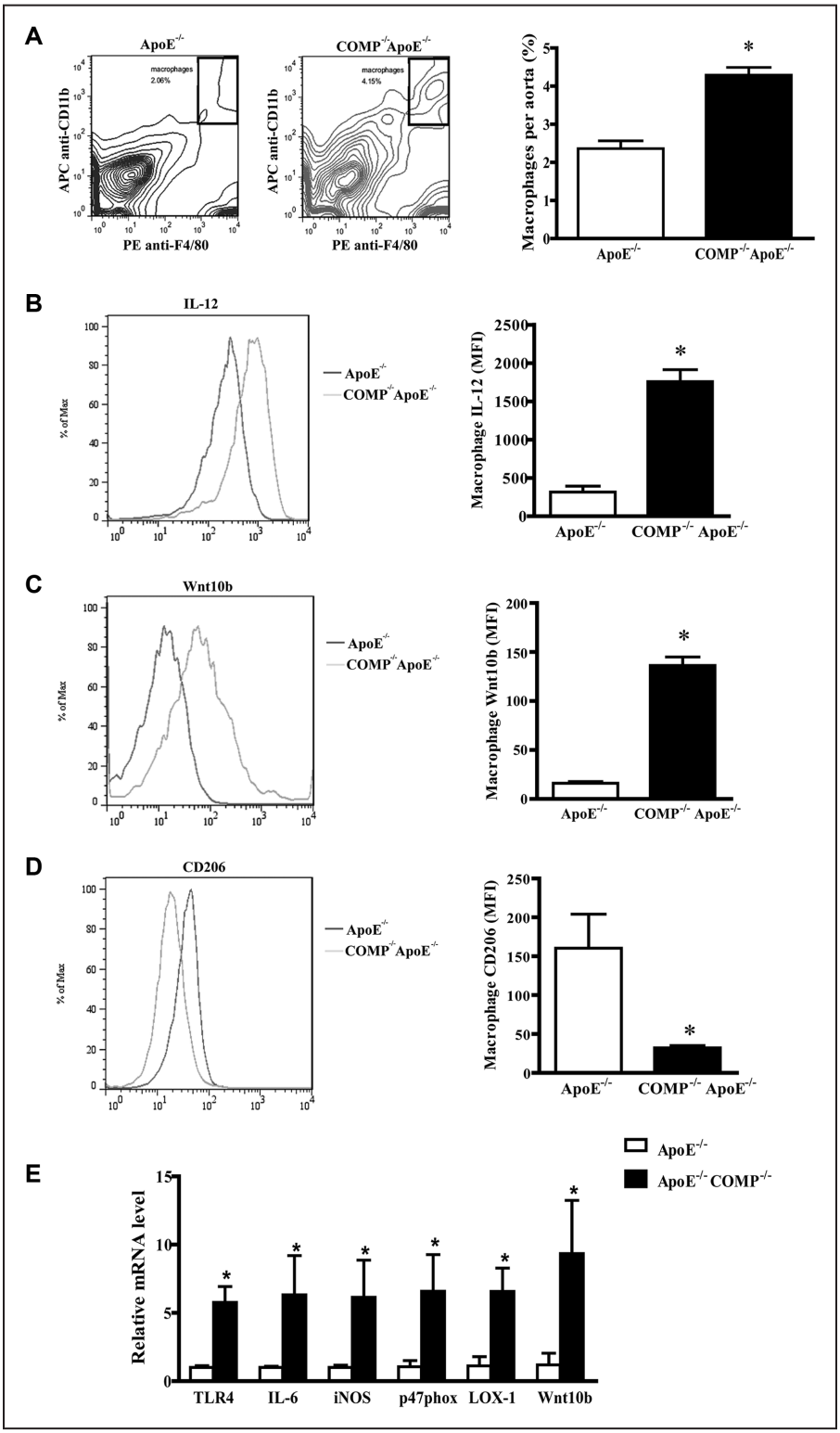

Figure 5. *COMP*$^{-/-}$ macrophages exhibit the atherogenic and osteogenic phenotype in atherosclerotic lesions. A, Representative flow cytometry results and quantification on percentages of macrophages in whole aortic single cells digested from *ApoE*$^{-/-}$ and *ApoE*$^{-/-}$*COMP*$^{-/-}$ mice. Flow cytometric measurement of interleukin (IL)-12 (**B**), Wnt10b (**C**), and CD206 (**D**) in gated macrophages from *ApoE*$^{-/-}$ and *ApoE*$^{-/-}$*COMP*$^{-/-}$ mice. Bar graph indicates the statistical analysis of mean fluorescent intensity (MFI). n=6; **P*<0.05. **E**, Relative mRNA measured and quantified via real-time polymerase chain reaction in lesional macrophages sorted from aortic tissues of *ApoE*$^{-/-}$ and *ApoE*$^{-/-}$*COMP*$^{-/-}$ mice by fluorescence-activated cell sorting. n=3; **P*<0.05. iNOS indicates inducible nitric oxide synthase; and TLR, toll-like receptor.

used for gating the macrophages and comparing the numbers of cells in the lesions (Figure 5A). Plaques from *ApoE*$^{-/-}$*COMP*$^{-/-}$ mice contained more macrophages than did plaques from *ApoE*$^{-/-}$ mice. IL-12 and Wnt10b were markedly increased in macrophages from lesions in *ApoE*$^{-/-}$*COMP*$^{-/-}$ mice, whereas the anti-inflammatory phenotype marker CD206 was greatly

decreased (Figure 5B–5D). Furthermore, we collected lesional macrophages from aortas of *ApoE*$^{-/-}$ and *ApoE*$^{-/-}$*COMP*$^{-/-}$ mice by fluorescence-activated cell sorting for evaluating mRNA expression. As shown in Figure 5E, macrophages from *ApoE*$^{-/-}$*COMP*$^{-/-}$ mice displayed the enhanced expression of TLR4, IL-6, iNOS, p47phox, LOX-1, and Wnt10b compared with the cells from *ApoE*$^{-/-}$ mice. Together, these findings indicate that COMP deficiency primes macrophages in plaques toward an atherogenic and osteogenic phenotype and may subsequently contribute to atherosclerotic calcification in vivo.

Integrin β3 Mediates the Phenotypic Shift in Macrophages Induced by COMP Deficiency

Integrins are recognized as cell surface receptors for matrix proteins and mediate the transduction of signals across the plasma membrane. We have reported that integrin β1 binds directly to COMP, whereas α7β1 mediates the effect of COMP on the phenotype of VSMCs.[22,31] Integrins α5β1 and αVβ3 mediate the attachment of chondrocytes to COMP.[32] Moreover, previous studies have indicated that integrin β3 deficiency macrophages aggravated atherosclerosis[33] and promoted osteosclerosis or osteopetrosis,[34] consistent with the phenotype of *COMP*$^{-/-}$ macrophages. To test whether integrin β1 or β3 mediates the role of COMP in inducing the phenotypic switch in macrophages, we first measured the levels of integrin β1 and β3 mRNA. COMP deficiency had no effect on the expression of integrin β1 or β3 mRNA (Online Figure XIA). In contrast, the level of integrin β3 protein, but not integrin β1 protein, was decreased in COMP-deficient macrophages (Online Figure XIB). Decreased protein expression of integrin β3 was verified in plaque macrophages from *ApoE*$^{-/-}$*COMP*$^{-/-}$ mice compared with those from *ApoE*$^{-/-}$ littermates fed with chow diet (Online Figure XIC). To address whether repressed integrin β3 expression mediated the effects of COMP deficiency, we overexpressed integrin β3 in *COMP*$^{-/-}$ macrophages. As shown in Online Figure XID–XII, overexpression of integrin β3 inhibited the COMP deficiency–induced increases in the expression of genes related to inflammation (TLR4 and IL-6), reactive oxygen species production (iNOS and p47phox), lipid uptake (LOX-1), and osteogenesis (Wnt10b). Consistent with this finding, the aggravation of VSMC calcium deposition by *COMP*$^{-/-}$ macrophages was rescued by overexpression of integrin β3 in macrophages (Figure 6A). To evaluate the role of integrin β3 in vivo, we transduced adeno-associated virus (AAV2)-green fluorescent protein (GFP) or AAV2–integrin β3 into 7-month-old *ApoE*$^{-/-}$*COMP*$^{-/-}$ mice. After 4-week Western-type diet feeding, peritoneal macrophages were isolated for detecting the efficiency of AAV infection. Flow cytometry demonstrated that 19.3% macrophages were infected with AAV2-GFP (Online Figure XIIA). The overexpression of integrin β3 in macrophages after AAV2–integrin β3 infection was validated by real-time polymerase chain reaction and Western blot (Online Figure XIIB and XIIC). There were no differences in body weight and serum lipids between these 2 groups of infected mice (Online Table VI). We analyzed atherosclerotic lesion and plaque composition by Movat pentachrome staining. Mice infected with AAV2–integrin β3 showed attenuated plaque area (Online Figure XIID) and diminished percentages of cartilaginous metaplasia, area containing chondrocyte-like cells and necrotic core area (Figure 6B–6E). Moreover, we evaluated the gene expression of lesional macrophages isolated from aortas via fluorescence-activated cell sorting. As shown in Figure 6F, overexpression of integrin β3 in lesional macrophages via AAV2 transfusion inhibited COMP deficiency–enhanced IL-6, p47phox, LOX-1, and Wnt10b expression. Thus, integrin β3 mediated the atherogenic and osteogenic phenotype induced in macrophages by COMP deficiency in vitro and in vivo.

As we reported previously that COMP knockdown induces VSMC dedifferentiation,[21] which also contributed to vascular calcification, we asked if integrin β3 in VSMCs mediated COMP deficiency–enhanced dedifferentiation. We measured integrin β3 in VSMCs after COMP silencing by real-time polymerase chain reaction and Western blot. There were no changes at both mRNA and protein levels (Online Figure XIIIA and XIIIB). Next, we asked whether overexpression of integrin β3 could reverse COMP silencing–induced VSMC phenotypic switching, similar to that integrin β3 blocked the effect of COMP deficiency in macrophages. However, integrin β3 overexpression seemed not affecting the decrement of VSMC contractile genes (SM-22α, α-actin, and calponin) induced by COMP silencing (Online Figure XIIIC–XIIIE). These results indicated the COMP–integrin β3 axis in macrophages but not in VSMCs is involved in atherosclerotic calcification.

COMP Binds Directly to Integrin β3 in Macrophages

To investigate further how COMP regulates integrin β3, we first performed coimmunoprecipitation experiments in peritoneal macrophages. As shown in Figure 7A, integrin β3 was immunoprecipitated by anti-COMP antibodies but not by rabbit IgG. Notably, COMP could also be exclusively immunoprecipitated by anti-integrin β3 antibodies (Figure 7B). This finding implies that COMP binds to integrin β3 in macrophages. Next, a mammalian 2-hybrid assay was used to identify the domains at which COMP and integrin β3 bind. To identify the potential COMP-binding motif within integrin β3, we generated pBIND plasmids subcloning the following distinct domains of integrin β3: aa 1 to 461 (hybrid and PSI [plexin-semaphorin-integrin] domains), aa 462 to 628 (epidermal growth factor repeats), aa 629 to 717 (β-tail domain), and aa 718 to 787 (transmembrane and cytoplasmic domains). These pBIND plasmids were cotransfected with a pACT vector with full-length COMP into COS-7 cells. Only the membrane-proximal β-tail domain bound to COMP (Figure 7C). In addition, to identify the integrin β3–binding motif in COMP, we subcloned various domains of COMP (N terminus, EGF repeats, type III repeats, and C terminus) into pACT plasmids. The constructs were coexpressed with the β-tail domain of the integrin β3–fused pBIND plasmid into COS-7 cells. The dual luciferase reporter assay revealed that the C-terminal domain of COMP and full-length COMP bound to the integrin β3 β-tail domain (Figure 7D). Thus, integrin β3 was identified as a COMP-binding protein in macrophages.

Blocking Binding Between COMP and Integrin β3 Primes Macrophages to Adopt an Atherogenic and Osteogenic Phenotype

To further address whether COMP–integrin β3 binding is essential for regulating macrophage phenotype, the β-tail domain

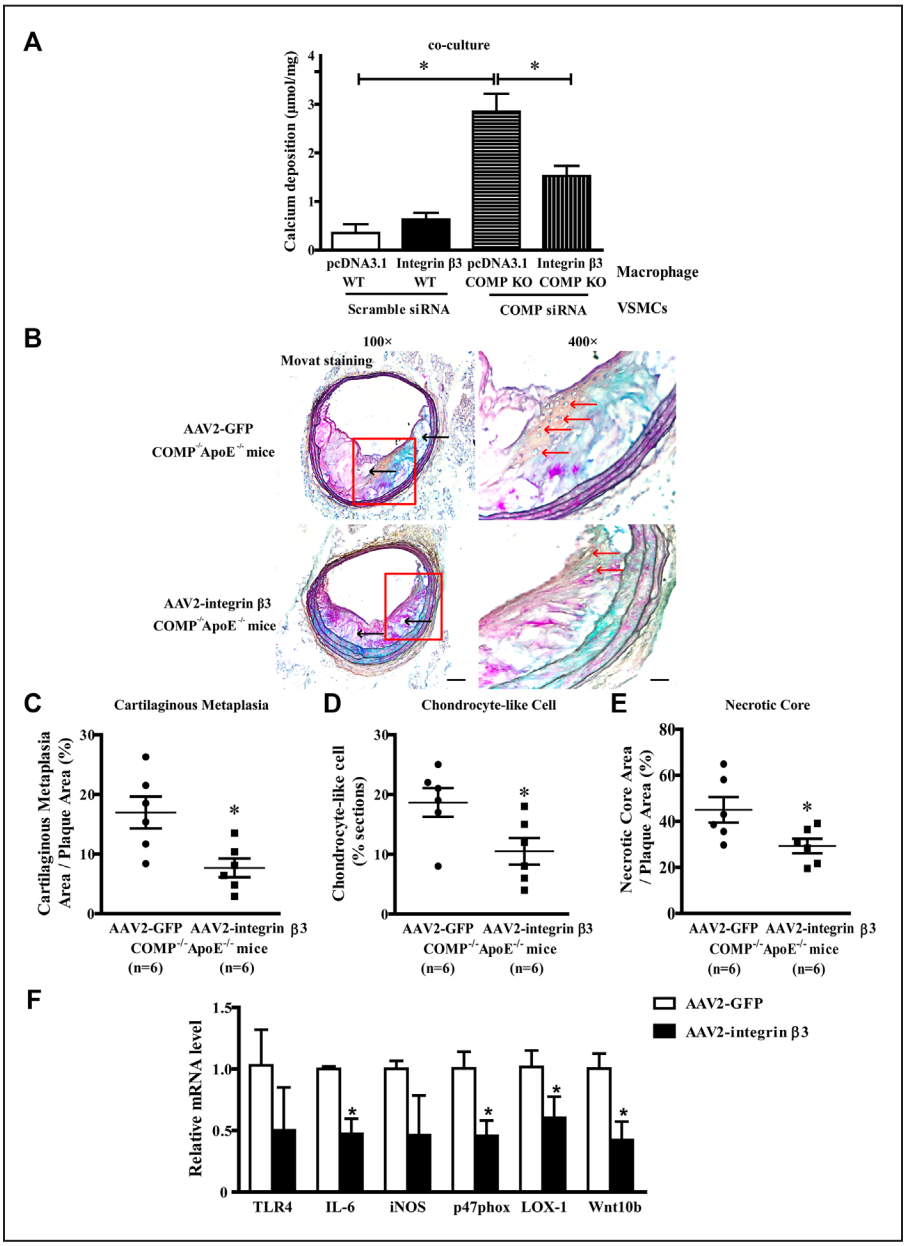

Figure 6. Integrin β3 mediates the phenotypic shift of macrophages and atherosclerotic calcification induced by cartilage oligomeric matrix protein (COMP) deficiency. A, A7r5 vascular smooth muscle cells (VSMCs) with or without COMP knockdown by small interfering RNA (siRNA) were cultured with conditioned medium from transfected macrophages for 12 days followed by measurement and quantification of calcium deposition. Three independent experiments were performed in duplicate. n=3; **P*<0.05. **B**, Representative images of Movat staining on cross sections of innominate arteries from 7-month-old *ApoE*$^{-/-}$*COMP*$^{-/-}$ mice injected with adeno-associated virus (AAV2)-GFP or AAV2–integrin β3 followed by 4-week Western-type diet feeding. Black arrows indicate necrotic core, whereas red arrows indicate chondrocyte-like cells in Movat staining. Scale bar, 100 μm (100×) and 20 μm (400×). Statistical analysis in the percentages of cartilaginous metaplasia area (**C**), plaque-containing chondrocyte-like cells (**D**), and necrotic core area (**E**) in atherosclerotic lesion. **P*<0.05. **F**, Relative mRNA was measured and quantified via real-time polymerase chain reaction in lesional macrophages sorted by fluorescence-activated cell sorting from aortic tissues of *ApoE*$^{-/-}$*COMP*$^{-/-}$ mice injected with AAV2-GFP or AAV2-integrin β3 followed by 4-week Western-type diet feeding. n=3; **P*<0.05. KO indicates knockout; IL, interleukin; iNOS, inducible nitric oxide synthase; TLR, toll-like receptor; and WT, wild-type.

of integrin β3 was used as a dominant negative fragment and transfected into macrophages to block the binding between COMP and integrin β3 (Online Figure XIVA). Transfection of the β-tail domain plasmid significantly reduced the protein level of integrin β3 in control macrophages, which are greatly similar to *COMP*$^{-/-}$ macrophages (Figure 7E). Moreover, interrupting binding between COMP and integrin β3 promoted the expression of TLR4, IL-6, iNOS, p47phox, LOX-1, and Wnt10b in WT macrophages (Figure 7F), mimicking the effects of COMP deficiency in macrophages. Furthermore, we transduced AAV2-GFP or AAV2-β-tail domain into 4-month-old *ApoE*$^{-/-}$ mice, respectively. The overexpression of β-tail domain in macrophages was confirmed by real-time polymerase chain reaction (Online Figure XIVB). Coinciding with

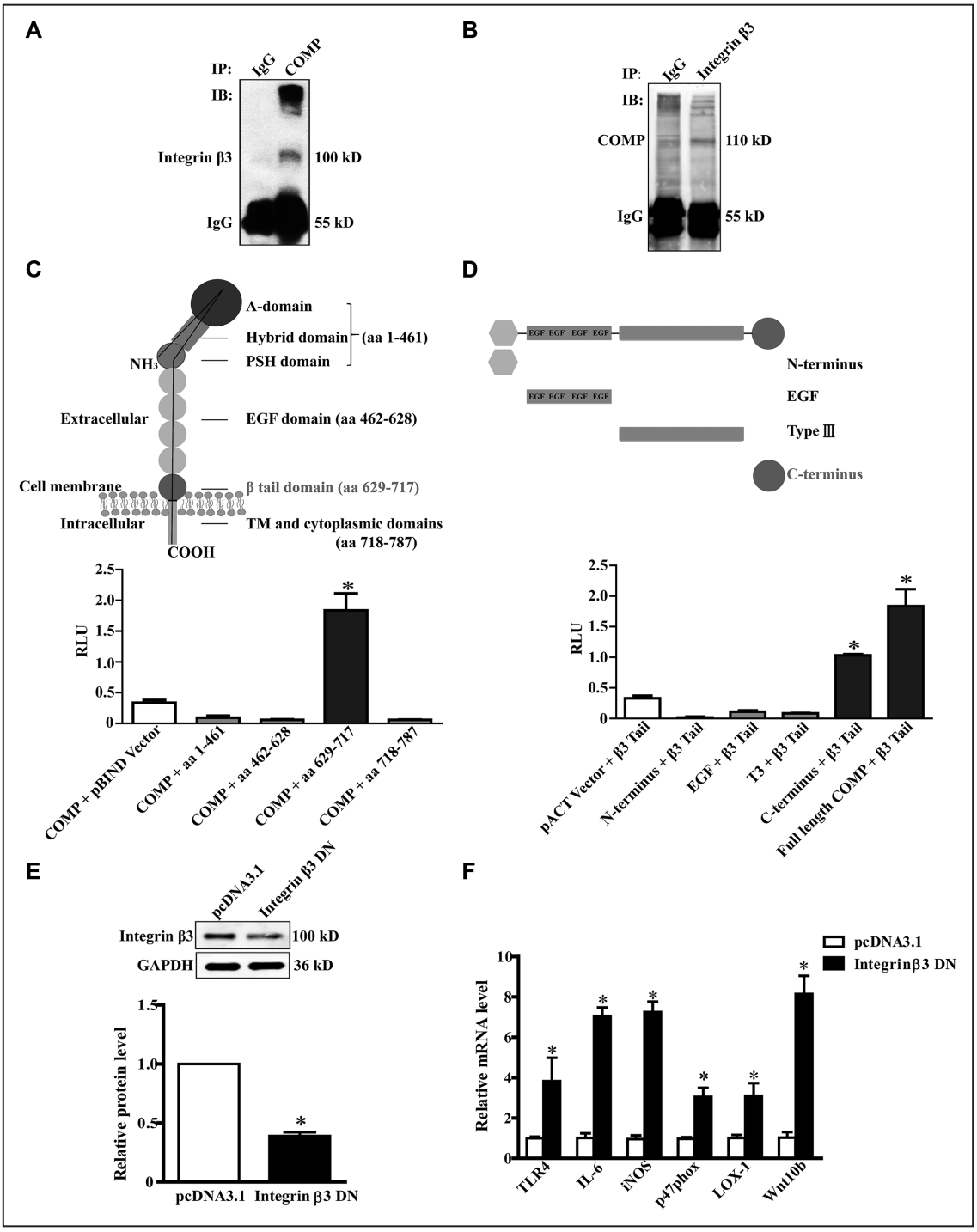

Figure 7. Cartilage oligomeric matrix protein (COMP) binds directly to integrin β3 in macrophages. A and **B**, Coimmunoprecipitation (IP) of COMP and integrin β3 in mouse peritoneal macrophages. Rabbit IgG was used as a negative control for IP. **C**, **Top**, Schematic illustration of integrin β1 constructs used to map corresponding domains (A-domain, hybrid and PSI [plexin-semaphorin-integrin] domains [aa 1–461], epidermal growth factor [EGF] repeats [aa 462–628], β-tail [aa 629–717], and transmembrane [TM] and cytoplasmic domains [aa 718–787]) that bind to COMP. The presence of binding between integrin β3 domains and COMP is indicated in light grey font. **Bottom**, Mammalian 2-hybrid analysis of interaction between integrin β3 and COMP. Luciferase activity assay of COS-7 cells transiently transfected for 48 h with domains of integrin β3 cloned into the pBIND vector, together with full-length COMP subcloned into the pACT vector. **D**, **Top**, Schematic illustration of COMP constructs used to map the corresponding domains (N-terminus, EGF, type III, and C-terminus) that bind to the integrin β3 β-tail domain. The presence of binding between COMP domains and the integrin β3 β-tail is indicated in light grey font. **Bottom**, Mammalian 2-hybrid analysis of COMP–integrin β3 domain interaction. Luciferase activity assay of COS-7 cells transiently transfected for 48 h with various domains of COMP cloned into pACT, together with the integrin β3 β-tail cloned into pBIND. Four independent experiments were performed in triplicate. n=4; **P*<0.05. **E**, Representative Western blot and quantification of integrin β3 expression in mouse peritoneal macrophages transfected with pcDNA3.1 or pcDNA3.1–integrin β3 dominant negative (DN) plasmids. **F**, Relative mRNA was measured and quantified in peritoneal macrophages with or without integrin β3 DN overexpression via real-time polymerase chain reaction. Three independent experiments were performed in duplicate. n=3; **P*<0.05. GAPDH indicates glyceraldehyde 3-phosphate dehydrogenase; IL, interleukin; iNOS, inducible nitric oxide synthase; RLU, relative light units; and TLR, toll-like receptor.

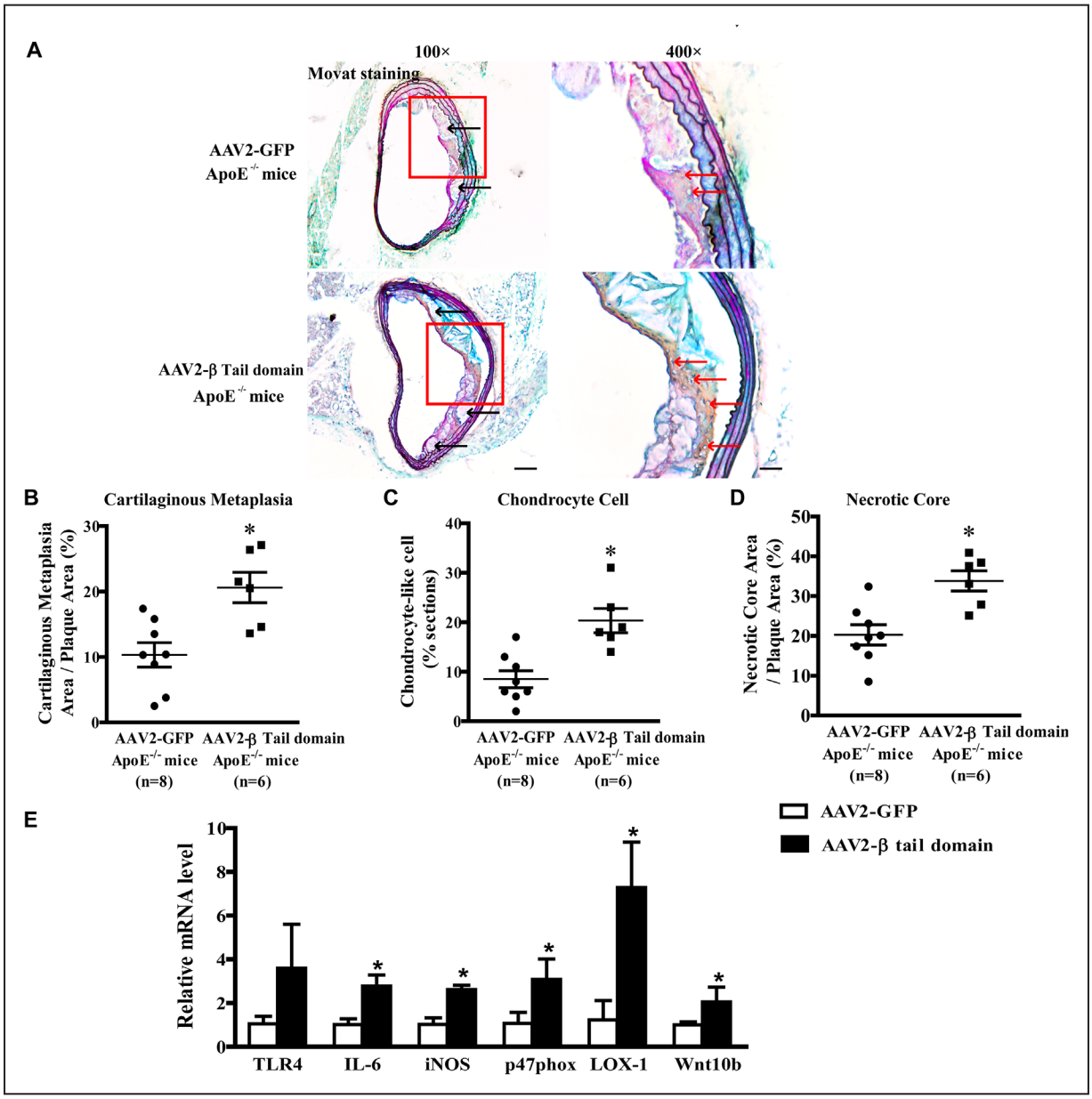

Figure 8. Cartilage oligomeric matrix protein (COMP)–integrin β3 interaction is involved in lesional macrophage phenotypic switching and atherosclerotic calcification. A, Representative images of Movat staining on cross sections of innominate arteries from 4-month-old *ApoE*$^{-/-}$ mice injected with adeno-associated virus (AAV2)-GFP or AAV2–β-tail domain followed by 4-week Western-type diet feeding. Black arrows indicate necrotic core, whereas red arrows indicate chondrocyte-like cells in Movat staining. Scale bar, 100 μm (100×) and 20 μm (400×). Statistical analysis in the percentages of cartilaginous metaplasia area (**B**), plaque-containing chondrocyte-like cells (**C**), and necrotic core area (**D**) in atherosclerotic lesion. **P*<0.05. **E**, Relative mRNA was measured and quantified via real-time polymerase chain reaction in lesional macrophages sorted by fluorescence-activated cell sorting from aortic tissues of *ApoE*$^{-/-}$ mice injected with AAV2-GFP or AAV2-β-tail domain followed by 4-week Western-type diet feeding. n=3; **P*<0.05. IL indicates interleukin; iNOS, inducible nitric oxide synthase; and TLR, toll-like receptor.

in vitro results, β-tail domain overexpression in macrophages of *ApoE*$^{-/-}$ mice decreased integrin β3 protein levels in vivo (Online Figure XIVC). There were no differences with regard to body weight and serum lipids between these 2 genotypes (Online Table VII). Atherosclerotic lesion and plaque composition analysis between AAV2-GFP–infected and AAV2-β-tail domain–infected *ApoE*$^{-/-}$ mice showed that overexpression of β-tail domain greatly enhanced atherosclerotic plaque (Online Figure XIVD) and markedly aggravated the percentages of cartilaginous metaplasia, area containing chondrocyte-like cells and necrotic core area (Figure 8A–8D). In addition, lesional macrophages with β-tail domain overexpression enhanced the expression of IL-6, iNOS, p47phox, LOX-1, and Wnt10b (Figure 8E). These provide supporting evidence that COMP modulates macrophage phenotypes through its interaction with integrin β3 in vitro and in vivo.

Discussion

The main finding of our study is that COMP deficiency accelerates atherosclerotic calcification in mice, which may

be associated with instability of atherosclerotic plaques. Intriguingly, COMP deficiency in macrophages drove the atherogenic and osteogenic phenotypic switch of macrophages in the lesion and may subsequently contribute to atherosclerotic calcification and plaque instability. Our study reveals the importance of this macrophage phenotypic shift in atherosclerotic calcification.

The contribution of macrophages to atherosclerotic calcification remains unclear. Previously, osteoclast-like cells, differentiated from hematopoietic precursors of the mononuclear phagocyte lineage, have been proposed to be able to remove artery wall mineral deposits for cell-based therapy because osteoclasts reduced the mineral content of calcified elastin in vitro[35] and because osteoclast-like cells in calcified atherosclerotic lesions from humans and mice are decreased after atherosclerotic calcification.[36] However, with the recognition of the osteoprotegerin/receptor activator of nuclear factor-κB triad/receptor activator of nuclear factor-κB ligand triad in calcification of the atheromatous plaques, contradictory results were reported. Knockout of osteoprotegerin, the inhibitor of receptor activator of nuclear factor-κB ligand–dependent osteoclast formation, leads to reduced lesion calcification.[37,38] Similarly, VSMC-specific knockout of Runx2 reduced the level of receptor activator of nuclear factor-κB ligand and subsequent osteoclast differentiation of macrophages and thereby inhibited atherosclerotic calcification.[14] However, all of these previous studies characterized the osteoclast-like macrophages in the lesions by using a few cell markers and not by expression profiling. Moreover, previous studies reported that proinflammatory macrophages were activated by lipid oxidation products and basic calcium phosphate crystals during atherosclerotic calcification.[11] The secretion of proinflammatory cytokines (TNF-α, IL-1, and IL-8) or matrix vesicles by activated macrophages has been suggested to be involved in atherosclerotic calcification.[11,20] However, the subtypes of macrophages activated during lesional calcification have not been fully characterized. Here, we analyzed the mRNA profile of *COMP*$^{-/-}$ macrophages and compared it with the existing gene array data for various macrophage subtypes. Our study revealed that gene expression by COMP-deficient macrophages positively correlated with that of M1, M2b, and Mox cells (the proinflammatory/atherogenic phenotypes) but negatively correlated with that of M2c macrophages and osteoclasts (the anti-inflammatory and antiosteogenic phenotypes). Further flow cytometric measurements confirmed that the profile of *COMP*$^{-/-}$ macrophages shifted toward proinflammatory and pro-osteogenic phenotypes, which is consistent with the observation from earlier in vivo molecular imaging.[39] Together with the chimeric bone marrow transplantation in vivo, these studies highlight the importance of a macrophage phenotype switch regulated by COMP during atherosclerotic calcification.

We have previously reported that COMP inhibits medial VSMC calcification by direct antagonism of bone morphogenetic protein 2.[22] In this study, we further revealed a novel role of COMP in inhibiting atherosclerotic calcification by regulating a macrophage phenotypic switch. Interestingly, COMP deficiency in bone marrow of donor mice rather than in recipient mice confers lesion calcification, whereas VSMC-specific *COMP*-Tg displayed no effect on cartilaginous metaplasia, indicating that bone marrow–derived cells seem more important in intimal calcification. Our data also reinforce the idea that although intimal and medial calcification show some coincidence and overlap, they differ in terms of risk factors, topography, molecular cascades, and clinical consequences. On the other hand, our study revealed that intimal calcification is not paralleled with atherosclerotic lesion as evidenced that *ApoE*$^{-/-}$ *COMP*$^{-/-}$ mice transplanted with bone marrow from *ApoE*$^{-/-}$ donor exhibited heavier plaque area but not calcification compared with *ApoE*$^{-/-}$ chimeric mice, as well as SMC *COMP*-Tg *ApoE*$^{-/-}$ mice exhibited the attenuated atherosclerotic lesions but identical cartilaginous metaplasia compared with *ApoE*$^{-/-}$ mice. In parallel, the *ApoE*$^{-/-}$ mice transplanted with bone marrow from *ApoE*$^{-/-}$*COMP*$^{-/-}$ donor but not *ApoE*$^{-/-}$*COMP*$^{-/-}$ mice receiving bone marrow from *ApoE*$^{-/-}$ mice showed more extensive necrotic core compared with *ApoE*$^{-/-}$ chimera although both groups manifested greater atherosclerotic lesion. Our results are consistent with recent studies that proinflammatory calcification proceeds vulnerable plaque.[7] The role of COMP in atherosclerosis was in line with previous observation.[40] The study reported that COMP deficiency increased the brachiocephalic lesions but had no effects on the carotid lesions by periadventitial cast injury of carotid artery in 14-week high fat-fed *ApoE*$^{-/-}$ mice. However, neither lesions in other atheroprone locations, including the aortic root and arch, nor the cellular origins of COMP were investigated in that study.

Our finding that the most severe intimal calcification was observed when COMP was absent from both vessel and bone marrow further raised the important issue of macrophage/VSMC cross talk in atherosclerotic calcification. Previous studies have shown that macrophages were activated by oxidative low-density lipoprotein–stimulated calcifying vascular cell mineralization via cell–cell interaction and the production of soluble factors.[11] Other reports have indicated roles for activated macrophages in high-phosphate or β-glycerophosphate–stimulated VSMC calcification.[41,42] Our study, however, used a coculture system with macrophages and VSMCs in the absence of stimulators. Even without high-phosphate stimulation, *COMP*$^{-/-}$ macrophages stimulated calcification of normal VSMCs. This effect was further aggravated when COMP was absent from both macrophages and VSMCs, indicating that these 2 cells have a synergistic effect in lesion calcification. It is well recognized that osteogenic factors released from macrophages can promote osteogenic process.[12] Conditioned medium from macrophages with elevated expression of Wnt10b, BMP-6, and SPHK1 (which catalyzes the phosphorylation of sphingosine to form S1P) could stimulate human mesenchymal stem cell migration and differentiation into the osteoblast lineage as evidenced by mineralized nodule formation in vitro, whereas conditioned medium containing the Wnt antagonist Dkk1, neutralizing antibodies against BMP-6, TNF-α, and IL-6, and an S1P antagonist blocked further osteoblast differentiation.[10] Here, we showed that COMP deficiency increased the expression of proinflammatory cytokines (such as IL-6 and

TNF-α) and osteogenic factors (such as Wnt10b) in macrophages in vitro and in vivo and in turn stimulated VSMC calcification. Of interest, SMC *COMP*-Tg inhibited medial calcification in ex vivo aortic rings but had no effect on intimal calcification in *ApoE*$^{-/-}$ mice. The possible reason for this distinct function of VSMC-derived COMP may be because of the various cellular compositions in different calcification sites, as well as VSMC phenotypic switching. VSMCs constitute the major cell type of vascular media and mainly determine the fate of medial calcification. In contrast, intimal calcification involves complex cellular components. The macrophage percentage in atherosclerotic lesion is much greater than that of VSMCs (43.4%–62.7% versus 8.1%–9.3%).[43] More recent lineage tracing studies further revealed that a portion of macrophage-like cells within intimal plaques originated from VSMCs through dedifferentiating while losing contractile VSMC markers, and this switching directly promotes atherosclerosis.[44,45] Thus, although our in vitro data indicated that both VSMCs and macrophage deficiency of COMP promoted VSMC calcification in coculture model, our chimeric mice model and SMC *COMP*-Tg data suggest that COMP deficiency in macrophages may play a more important role in lesional calcification than lacking of COMP in VSMCs.

Herein, we reported that COMP deficiency modulated macrophage phenotypes through integrin β3 in vitro and in vivo. Integrin β3 deficiency in macrophages has been reported to aggravate atherosclerotic lesions by enhancing the macrophage inflammatory phenotype,[33] which was consistent with the effects of COMP deficiency in macrophages. Overexpression of integrin β3 in COMP-deficient macrophages prevented the enhanced inflammation, reactive oxygen species production, and low-density lipoprotein uptake, whereas the atherogensis was also attenuated in *ApoE*$^{-/-}$*COMP*$^{-/-}$ mice by injection of AAV2–integrin β3. Furthermore, integrin β3 deficiency in osteoclasts decreased their suppressive effect on osteogenesis and instead promoted osteosclerosis or osteopetrosis,[34] indicating that integrin β3 deficiency in macrophages contributed to osteogenesis. This was further emphasized by our data showing that overexpression of integrin β3 in COMP-deficient macrophages reversed the increases in Wnt10b expression and VSMC calcification, whereas blocking COMP–integrin β3 interaction by overexpression of β-tail domain in WT macorphage phenocopied the *COMP*$^{-/-}$ cells. We further confirmed in in vivo experiments that cartilaginous metaplasia was inhibited in *ApoE*$^{-/-}$*COMP*$^{-/-}$ mice transduced with AAV2–integrin β3 but enhanced in *ApoE*$^{-/-}$ mice infected with AAV2–β-tail domain. Thus, these data highlight the importance of the COMP–integrin β3 axis in modulating macrophage phenotypes and atherosclerotic calcification. Besides integrin β3, whether other molecules also mediated COMP deficiency–aggravated atherosclerotic calcification needs further investigation. We previously reported that COMP is a natural inhibitor of thrombin and its deficiency in bone marrow accelerated hemostasis and thrombosis in mice,[46] indicating that bone marrow–derived COMP also inhibits hemostasis and thrombosis. To date, there is no report on the direct association between thrombin and atherosclerotic calcification, but thrombin was reported to cleave the anticalcific factor osteopontin.[47] Thus, whether the inhibitory effect of COMP on thrombin is involved in atherosclerotic calcification may need further studies. We also measured COMP in mice plasma after bone marrow transplantation by ELISA (Online Table III). As a result, both COMP deficiency in bone marrow and non–bone marrow tissues attenuated the plasma level of COMP, but COMP deficiency in bone marrow even exhibited a more significant attenuation of plasma COMP as evidenced by that the plasma COMP in *ApoE*$^{-/-}$ mice receiving *ApoE*$^{-/-}$*COMP*$^{-/-}$ bone marrow was lower than the plasma levels in *ApoE*$^{-/-}$*COMP*$^{-/-}$ mice transplanted with *ApoE*$^{-/-}$ bone marrow. To explore the possible role of circulating COMP in atherosclerotic calcification, further investigation might be needed.

In conclusion, COMP deficiency drove macrophages toward an atherogenic and osteogenic phenotype to promote atherosclerotic calcification via suppressing integrin β3. Thus, the application of the extracellular matrix protein COMP to modulate macrophage phenotypes may be a potential therapeutic method for ameliorating atherogenesis, atherosclerotic calcification, and plaque rupture.

Acknowledgments

We appreciated Dr Ake Oldberg from Lund University for kindly providing *COMP*$^{-/-}$ mice for our in vivo experiments, Dr Guang Hu from National Institute of Environmental Health Science for generously providing short hairpin RNA lentivirus cloning and package vectors, and Dr Jing Zhou from Peking University for offering BAECs (bovine aortic endothelial cells) for our transmigration experiments.

Sources of Funding

This research was supported by funding from the National Natural Science Foundation (NSFC) of the P. R. China (91539203, 81070243, and 81121061); the National Program on Key Basic Research Projects (973 Program) (2010CB912504 and 2012CB518002); the National Science Fund for distinguished Young Scholars (81225002); International Cooperation and Exchanges NSFC (81220108004); the 111 Project of Chinese Ministry of Education (no. B07001); National Science Fund for Young Scholars (81300198); and Specialized Research Fund for the Doctoral Program of Higher Education (20130001120026).

Disclosures

None.

References

1. Sage AP, Tintut Y, Demer LL. Regulatory mechanisms in vascular calcification. *Nat Rev Cardiol*. 2010;7:528–536. doi: 10.1038/nrcardio.2010.115.
2. Wu M, Rementer C, Giachelli CM. Vascular calcification: an update on mechanisms and challenges in treatment. *Calcif Tissue Int*. 2013;93:365–373. doi: 10.1007/s00223-013-9712-z.
3. Johnson RC, Leopold JA, Loscalzo J. Vascular calcification: pathobiological mechanisms and clinical implications. *Circ Res*. 2006;99:1044–1059. doi: 10.1161/01.RES.0000249379.55535.21.
4. Lanzer P, Boehm M, Sorribas V, Thiriet M, Janzen J, Zeller T, St Hilaire C, Shanahan C. Medial vascular calcification revisited: review and perspectives. *Eur Heart J*. 2014;35:1515–1525. doi: 10.1093/eurheartj/ehu163.
5. Demer LL, Tintut Y. Inflammatory, metabolic, and genetic mechanisms of vascular calcification. *Arterioscler Thromb Vasc Biol*. 2014;34:715–723. doi: 10.1161/ATVBAHA.113.302070.

6. Irkle A, Vesey AT, Lewis DY, Skepper JN, Bird JL, Dweck MR, Joshi FR, Gallagher FA, Warburton EA, Bennett MR, Brindle KM, Newby DE, Rudd JH, Davenport AP. Identifying active vascular microcalcification by (18)F-sodium fluoride positron emission tomography. *Nat Commun*. 2015;6:7495. doi: 10.1038/ncomms8495.
7. Pugliese G, Iacobini C, Blasetti Fantauzzi C, Menini S. The dark and bright side of atherosclerotic calcification. *Atherosclerosis*. 2015;238:220–230. doi: 10.1016/j.atherosclerosis.2014.12.011.
8. Naik V, Leaf EM, Hu JH, Yang HY, Nguyen NB, Giachelli CM, Speer MY. Sources of cells that contribute to atherosclerotic intimal calcification: an in vivo genetic fate mapping study. *Cardiovasc Res*. 2012;94:545–554. doi: 10.1093/cvr/cvs126.
9. Bennett CN, Ouyang H, Ma YL, Zeng Q, Gerin I, Sousa KM, Lane TF, Krishnan V, Hankenson KD, MacDougald OA. Wnt10b increases postnatal bone formation by enhancing osteoblast differentiation. *J Bone Miner Res*. 2007;22:1924–1932. doi: 10.1359/jbmr.070810.
10. Pederson L, Ruan M, Westendorf JJ, Khosla S, Oursler MJ. Regulation of bone formation by osteoclasts involves Wnt/BMP signaling and the chemokine sphingosine-1-phosphate. *Proc Natl Acad Sci U S A*. 2008;105:20764–20769. doi: 10.1073/pnas.0805133106.
11. Tintut Y, Patel J, Territo M, Saini T, Parhami F, Demer LL. Monocyte/macrophage regulation of vascular calcification in vitro. *Circulation*. 2002;105:650–655. doi: 10.1161/hc0502.102969.
12. Bessueille L, Magne D. Inflammation: a culprit for vascular calcification in atherosclerosis and diabetes. *Cell Mol Life Sci*. 2015;72:2475–2489. doi: 10.1007/s00018-015-1876-4.
13. Shao JS, Cheng SL, Sadhu J, Towler DA. Inflammation and the osteogenic regulation of vascular calcification: a review and perspective. *Hypertension*. 2010;55:579–592. doi: 10.1161/HYPERTENSIONAHA.109.134205.
14. Sun Y, Byon CH, Yuan K, Chen J, Mao X, Heath JM, Javed A, Zhang K, Anderson PG, Chen Y. Smooth muscle cell-specific runx2 deficiency inhibits vascular calcification. *Circ Res*. 2012;111:543–552. doi: 10.1161/CIRCRESAHA.112.267237.
15. Vattikuti R, Towler DA. Osteogenic regulation of vascular calcification: an early perspective. *Am J Physiol Endocrinol Metab*. 2004;286:E686–E696. doi: 10.1152/ajpendo.00552.2003.
16. Massy ZA, Mentaverri R, Mozar A, Brazier M, Kamel S. The pathophysiology of vascular calcification: are osteoclast-like cells the missing link? *Diabetes Metab*. 2008;34(suppl 1):S16–S20. doi: 10.1016/S1262-3636(08)70098-3.
17. Simpson CL, Lindley S, Eisenberg C, Basalyga DM, Starcher BC, Simionescu DT, Vyavahare NR. Toward cell therapy for vascular calcification: osteoclast-mediated demineralization of calcified elastin. *Cardiovasc Pathol*. 2007;16:29–37. doi: 10.1016/j.carpath.2006.07.001.
18. Collin-Osdoby P. Regulation of vascular calcification by osteoclast regulatory factors RANKL and osteoprotegerin. *Circ Res*. 2004;95:1046–1057. doi: 10.1161/01.RES.0000149165.99974.12.
19. Preusch MR, Rattazzi M, Albrecht C, Merle U, Tuckermann J, Schütz G, Blessing E, Zoppellaro G, Pauletto P, Krempien R, Rosenfeld ME, Katus HA, Bea F. Critical role of macrophages in glucocorticoid driven vascular calcification in a mouse-model of atherosclerosis. *Arterioscler Thromb Vasc Biol*. 2008;28:2158–2164. doi: 10.1161/ATVBAHA.108.174128.
20. New SE, Goettsch C, Aikawa M, Marchini JF, Shibasaki M, Yabusaki K, Libby P, Shanahan CM, Croce K, Aikawa E. Macrophage-derived matrix vesicles: an alternative novel mechanism for microcalcification in atherosclerotic plaques. *Circ Res*. 2013;113:72–77. doi: 10.1161/CIRCRESAHA.113.301036.
21. Wang L, Zheng J, Du Y, Huang Y, Li J, Liu B, Liu CJ, Zhu Y, Gao Y, Xu Q, Kong W, Wang X. Cartilage oligomeric matrix protein maintains the contractile phenotype of vascular smooth muscle cells by interacting with alpha(7)beta(1) integrin. *Circ Res*. 2010;106:514–525. doi: 10.1161/CIRCRESAHA.109.202762.
22. Du Y, Wang Y, Wang L, Liu B, Tian Q, Liu CJ, Zhang T, Xu Q, Zhu Y, Ake O, Qi Y, Tang C, Kong W, Wang X. Cartilage oligomeric matrix protein inhibits vascular smooth muscle calcification by interacting with bone morphogenetic protein-2. *Circ Res*. 2011;108:917–928. doi: 10.1161/CIRCRESAHA.110.234328.
23. Wang L, Zheng J, Bai X, Liu B, Liu CJ, Xu Q, Zhu Y, Wang N, Kong W, Wang X. ADAMTS-7 mediates vascular smooth muscle cell migration and neointima formation in balloon-injured rat arteries. *Circ Res*. 2009;104:688–698. doi: 10.1161/CIRCRESAHA.108.188425.
24. Du Y, Gao C, Liu Z, Wang L, Liu B, He F, Zhang T, Wang Y, Wang X, Xu M, Luo GZ, Zhu Y, Xu Q, Wang X, Kong W. Upregulation of a disintegrin and metalloproteinase with thrombospondin motifs-7 by miR-29 repression mediates vascular smooth muscle calcification. *Arterioscler Thromb Vasc Biol*. 2012;32:2580–2588. doi: 10.1161/ATVBAHA.112.300206.
25. Aherrahrou Z, Schunkert H. Genetics of atherosclerosis and vascular calcification go hand-in-hand. *Atherosclerosis*. 2013;228:325–326. doi: 10.1016/j.atherosclerosis.2012.10.029.
26. Reilly MP, Li M, He J, et al; Myocardial Infarction Genetics Consortium; Wellcome Trust Case Control Consortium. Identification of ADAMTS7 as a novel locus for coronary atherosclerosis and association of ABO with myocardial infarction in the presence of coronary atherosclerosis: two genome-wide association studies. *Lancet*. 2011;377:383–392. doi: 10.1016/S0140-6736(10)61996-4.
27. van Setten J, Isgum I, Smolonska J, et al. Genome-wide association study of coronary and aortic calcification implicates risk loci for coronary artery disease and myocardial infarction. *Atherosclerosis*. 2013;228:400–405. doi: 10.1016/j.atherosclerosis.2013.02.039.
28. Svensson L, Aszódi A, Heinegård D, Hunziker EB, Reinholt FP, Fässler R, Oldberg A. Cartilage oligomeric matrix protein-deficient mice have normal skeletal development. *Mol Cell Biol*. 2002;22:4366–4371. doi: 10.1128/MCB.22.12.4366-4371.2002.
29. Rattazzi M, Bennett BJ, Bea F, Kirk EA, Ricks JL, Speer M, Schwartz SM, Giachelli CM, Rosenfeld ME. Calcification of advanced atherosclerotic lesions in the innominate arteries of ApoE-deficient mice: potential role of chondrocyte-like cells. *Arterioscler Thromb Vasc Biol*. 2005;25:1420–1425. doi: 10.1161/01.ATV.0000166600.58468.1b.
30. Heinonen SE, Leppänen P, Kholová I, Lumivuori H, Häkkinen SK, Bosch F, Laakso M, Ylä-Herttuala S. Increased atherosclerotic lesion calcification in a novel mouse model combining insulin resistance, hyperglycemia, and hypercholesterolemia. *Circ Res*. 2007;101:1058–1067. doi: 10.1161/CIRCRESAHA.107.154401.
31. Huang Y, Xia J, Zheng J, Geng B, Liu P, Yu F, Liu B, Zhang H, Xu M, Ye P, Zhu Y, Xu Q, Wang X, Kong W. Deficiency of cartilage oligomeric matrix protein causes dilated cardiomyopathy. *Basic Res Cardiol*. 2013;108:374. doi: 10.1007/s00395-013-0374-9.
32. Chen FH, Thomas AO, Hecht JT, Goldring MB, Lawler J. Cartilage oligomeric matrix protein/thrombospondin 5 supports chondrocyte attachment through interaction with integrins. *J Biol Chem*. 2005;280:32655–32661. doi: 10.1074/jbc.M504778200.
33. Schneider JG, Zhu Y, Coleman T, Semenkovich CF. Macrophage beta3 integrin suppresses hyperlipidemia-induced inflammation by modulating TNFalpha expression. *Arterioscler Thromb Vasc Biol*. 2007;27:2699–2706. doi: 10.1161/ATVBAHA.107.153650.
34. McHugh KP, Hodivala-Dilke K, Zheng MH, Namba N, Lam J, Novack D, Feng X, Ross FP, Hynes RO, Teitelbaum SL. Mice lacking beta3 integrins are osteosclerotic because of dysfunctional osteoclasts. *J Clin Invest*. 2000;105:433–440. doi: 10.1172/JCI8905.
35. Thavarajah M, Evans DB, Kanis JA. 1,25(OH)2D3 induces differentiation of osteoclast-like cells from human bone marrow cultures. *Biochem Biophys Res Commun*. 1991;176:1189–1195. doi: 10.1016/0006-291X(91)90411-Y.
36. Doherty TM, Uzui H, Fitzpatrick LA, Tripathi PV, Dunstan CR, Asotra K, Rajavashisth TB. Rationale for the role of osteoclast-like cells in arterial calcification. *FASEB J*. 2002;16:577–582. doi: 10.1096/fj.01-0898hyp.
37. Bucay N, Sarosi I, Dunstan CR, Morony S, Tarpley J, Capparelli C, Scully S, Tan HL, Xu W, Lacey DL, Boyle WJ, Simonet WS. Osteoprotegerin-deficient mice develop early onset osteoporosis and arterial calcification. *Genes Dev*. 1998;12:1260–1268.
38. Callegari A, Coons ML, Ricks JL, Yang HL, Gross TS, Huber P, Rosenfeld ME, Scatena M. Bone marrow- or vessel wall-derived osteoprotegerin is sufficient to reduce atherosclerotic lesion size and vascular calcification. *Arterioscler Thromb Vasc Biol*. 2013;33:2491–2500. doi: 10.1161/ATVBAHA.113.301755.
39. Aikawa E, Nahrendorf M, Figueiredo JL, Swirski FK, Shtatland T, Kohler RH, Jaffer FA, Aikawa M, Weissleder R. Osteogenesis associates with inflammation in early-stage atherosclerosis evaluated by molecular imaging in vivo. *Circulation*. 2007;116:2841–2850. doi: 10.1161/CIRCULATIONAHA.107.732867.
40. Bond AR, Hultgårdh-Nilsson A, Knutsson A, Jackson CL, Rauch U. Cartilage oligomeric matrix protein (COMP) in murine brachiocephalic and carotid atherosclerotic lesions. *Atherosclerosis*. 2014;236:366–372. doi: 10.1016/j.atherosclerosis.2014.07.029.
41. Jono S, Nishizawa Y, Shioi A, Morii H. 1,25-Dihydroxyvitamin D3 increases in vitro vascular calcification by modulating secretion of endogenous parathyroid hormone-related peptide. *Circulation*. 1998;98:1302–1306. doi: 10.1161/01.CIR.98.13.1302.

42. Boyle JJ, Bowyer DE, Weissberg PL, Bennett MR. Human blood-derived macrophages induce apoptosis in human plaque-derived vascular smooth muscle cells by Fas-ligand/Fas interactions. *Arterioscler Thromb Vasc Biol*. 2001;21:1402–1407. doi: 10.1161/hq0901.094279.
43. Shiomi M, Ito T, Tsukada T, Yata T, Ueda M. Cell compositions of coronary and aortic atherosclerotic lesions in WHHL rabbits differ. An immunohistochemical study. *Arterioscler Thromb*. 1994;14:931–937. doi: 10.1161/01.ATV.14.6.931.
44. Shankman LS, Gomez D, Cherepanova OA, Salmon M, Alencar GF, Haskins RM, Swiatlowska P, Newman AA, Greene ES, Straub AC, Isakson B, Randolph GJ, Owens GK. KLF4-dependent phenotypic modulation of smooth muscle cells has a key role in atherosclerotic plaque pathogenesis. *Nat Med*. 2015;21:628–637. doi: 10.1038/nm.3866.
45. Bennett MR, Sinha S, Owens GK. Vascular smooth muscle cells in atherosclerosis. *Circ Res*. 2016;118:692–702. doi: 10.1161/CIRCRESAHA.115.306361.
46. Liang Y, Fu Y, Qi R, Wang M, Yang N, He L, Yu F, Zhang J, Yun CH, Wang X, Liu J, Kong W. Cartilage oligomeric matrix protein is a natural inhibitor of thrombin. *Blood*. 2015;126:905–914. doi: 10.1182/blood-2015-01-621292.
47. Breyne J, Juthier F, Corseaux D, Marechaux S, Zawadzki C, Jeanpierre E, Ung A, Ennezat PV, Susen S, Van Belle E, Le Marec H, Vincentelli A, Le Tourneau T, Jude B. Atherosclerotic-like process in aortic stenosis: activation of the tissue factor-thrombin pathway and potential role through osteopontin alteration. *Atherosclerosis*. 2010;213:369–376. doi: 10.1016/j.atherosclerosis.2010.07.047.

Novelty and Significance

What Is Known?

- Atherosclerotic calcification is highly correlated with atherosclerotic plaque burden.
- Cartilage oligomeric matrix protein (COMP) plays a protective role in vascular smooth muscle cell calcification.

What New Information Does This Article Contribute?

- COMP deficiency drives the development of atherosclerotic calcification.
- COMP deficiency primes lesional macrophages toward an atherogenic and osteogenic but not anti-inflammatory or osteoclast phenotype.
- COMP–integrin β3 interaction in macrophages but not in vascular smooth muscle cells plays an essential role in atherosclerotic calcification.

The role of macrophages in the pathogenesis of atherosclerotic calcification is poorly understood. Our study revealed that deficiency of the matricellular protein COMP in macrophages aggravates atherogenesis and atherosclerotic calcification. Mechanistically, COMP deficiency primes the atherogenic and osteogenic phenotype of macrophages because of the modulation of cell surface integrin β3 protein. Our study highlights the importance of a macrophage phenotype switch regulated by COMP during atherosclerotic calcification, which might be related to plaque instability. Thus, the application of COMP to drive the macrophage phenotypic switching may be a potential therapeutic approach for ameliorating atherogenesis, atherosclerotic calcification, and plaque rupture.

Circulation Research
JOURNAL OF THE AMERICAN HEART ASSOCIATION

Shift of Macrophage Phenotype Due to Cartilage Oligomeric Matrix Protein Deficiency Drives Atherosclerotic Calcification

Yi Fu, Cheng Gao, Ying Liang, Meili Wang, Yaqian Huang, Wei Ma, Tuoyi Li, Yiting Jia, Fang Yu, Wanlin Zhu, Qinghua Cui, Yanhui Li, Qingbo Xu, Xian Wang and Wei Kong

Circ Res. 2016;119:261-276; originally published online May 5, 2016;
doi: 10.1161/CIRCRESAHA.115.308021
Circulation Research is published by the American Heart Association, 7272 Greenville Avenue, Dallas, TX 75231

Print ISSN: 0009-7330. Online ISSN: 1524-4571

Supplemental Material

Methods

Materials

Antibodies against integrin β1 and β3 were obtained from Santa Cruz Biotechnology (Santa Cruz, CA, USA). The antibody against GAPDH was obtained from Cell Signaling Technology (Boston, MA, USA). The antibody against COMP was obtained from Abcam (Cambridge, UK). Antibody against Wnt10b was purchased from ABGENT (San Diego, CA, USA). Antibodies applied for flow cytometry were purchased from BioLegend (San Diego, CA, USA). Reconstituted mouse IL-4 and IFNγ were purchased from PeproTech (Rocky Hill, NJ, USA). Thioglycollate was purchased from BD Biosciences (San Diego, CA, USA). DiI-ac-LDL was obtained from Life Technologies (Grand Island, NY, USA). IRDye-conjugated secondary antibodies for western blotting were purchased from Rockland, Inc. (Gilbertsville, PA, USA). Other reagents were obtained from Sigma-Aldrich (St. Louis, MO, USA) unless specified.

Animals

All animal studies followed the guidelines of the Animal Care and Use Committee of Peking University. $COMP^{-/-}$ mice in the C57BL/6 background strain were kindly provided by Professor Oldberg Ake from the Department of Cell and Molecular Biology at Lund University, Sweden.[1] Eight-week-old $COMP^{-/-}$ mice and their wild-type (WT) littermates were used for cell isolations. $COMP^{-/-}$ mice were crossbred with $ApoE^{-/-}$ mice in the C57BL/6 background to produce $ApoE^{-/-}COMP^{-/-}$ mice. Twelve-month-old male $ApoE^{-/-}COMP^{-/-}$ mice and their $ApoE^{-/-}$ littermates were used for further experiments.

Measurement of Plasma Lipids and COMP

Mice were euthanized using CO_2, and blood was collected by cardiac puncture with EDTA as an anticoagulant. Blood cells were analyzed by flow cytometry. Plasma was isolated by centrifuging blood at 3,000 g for 20 min. Total plasma cholesterol levels and triglyceride were assayed with kits from Zhong Sheng Bio-technology (Beijing, China). COMP in plasma were measured via ELISA kit following the product user's manual (Immunodiagnotis systems, Bolden Business Park, United Kingdom).

Analysis of Atherosclerotic Plaques and Calcification

Mice were euthanized and lesions in the whole aortic tree and in frozen cross-sections of the aortic root, arch and innominate artery were analyzed separately as described in the previous studies.[2, 3] The whole aorta was exposed and the perivascular tissues were removed *in situ*. Subsequently, the aorta was completely isolated and further incisions were made following the ventral side of the aorta, the inner curvature of the aorta and the outer curvature of the arch. Then, the flattened aorta was fixed on a black wax surface in a dissecting pan for Oil Red O staining. For further morphometric analysis of lesions, cross-sections of various artery parts including aortic root, arch and innominate artery were prepared individually. Moving up from the base of heart, aortic root region begins at the first appearance of the valve cups dividing the lumen into three distinct regions, and ends when the valve cups no longer divide the lumen and the wall appears more rounded and distinct. Aortic arch region for lesion analysis starts at the branch point of innominate artery then moving backwards to the aortic root. Innominate artery

region begins at its origin on the outer curve of aortic arch and ends at its first branch which is divided as right common carotid artery and right subclavian artery. Every three continuous 7 μm thick sections were made on separate slides without interval for aortic root and with 70 μm intervals for aortic arch and innominate artery respectively with a cryostat through these arterial parts. For each mouse, three sets of ten intervals sections were applied for Oil Red O, von Kossa and Movat pentachrome stainings. Cross-sections were with Oil Red O to allow assessment of atherosclerotic plaques, and images were captured by microscopy.[4] Von Kossa staining was performed to detect atherosclerotic calcification.[2, 5] The frozen sections were incubated with 1% $AgNO_3$ under ultraviolet light for 20-60 min depending on the light intensity. Then, un-reacted silver was removed by incubation with 5% $Na_2S_2O_3$ for 5 min. Before mounting, sections were counterstained with DAPI to identify nuclei. Stained sections were imaged using an Olympus microscopy system and evaluated blindly by two independent investigators. The total lesion area and calcification area were quantified as the percentage of plaque or calcification area to artery lumen area in each section individually, and the mean percentage of ten sections was recorded as the lesion data for each mouse.

Movat pentachrome staining kit (Leagene Biotechnology, Beijing, China) were applied on the cross-sections of innominate artery for assessing the atherosclerotic necrotic core and cartilaginous metaplasia. Two independent investigators who were blinded to the study protocol evaluated each section. In atherosclerotic lesions, necrotic core indicated as the non-cellular area without significant staining. Cartilaginous metaplasia was defined as a collagen-(yellow) and proteoglycan-(blue) rich extracellular matrix embedded with chondrocyte-like cells visualized as relatively large amount of clear cytoplasm surrounded by a lacunae.[6, 7] Both of necrotic core and cartilaginous metaplasia were quantified as the mean percentages of their area to the respective plaque area from ten sections for each mouse.

Bone Marrow Transplantation

Bone marrow transplantation was performed as described in previous reports with minor modifications.[8, 9] Mice were exposed to γ-irradiation from ^{60}Co (Department of Applied Chemistry, Peking University) followed by the injection of bone marrow cells (5×10^6 cells/mice) via the tail vein. To confirm the lethal exposure dose, mice that did not receive bone marrow injections were used as controls. $ApoE^{-/-}$ mice (8 weeks old) were exposed to 9 Gy of γ-irradiation. Control mice died 2 weeks post-irradiation, whereas all engrafted mice survived. However, all $ApoE^{-/-}COMP^{-/-}$ mice that received bone marrow cells died following 9 Gy of irradiation. To avoid high mortality from engraftment, 4 Gy of γ-irradiation was applied twice at a 4-hour interval[10]. $ApoE^{-/-}COMP^{-/-}$ mice exposed to 2×4 Gy survived when injection with bone marrow cells, whereas all control mice died within 2 weeks. Nevertheless, 1/4 of the $ApoE^{-/-}$ control mice survived after 2×4 Gy exposure. Thus, 9 Gy of irradiation was used as the lethal dose for $ApoE^{-/-}$ mice, and 2×4 Gy was used for $ApoE^{-/-}COMP^{-/-}$ mice. Bone marrow cells prepared from tibias and femurs from donors including $ApoE^{-/-}$ and $ApoE^{-/-}COMP^{-/-}$ mice (4-6 weeks old) were injected via the tail vein into lethally irradiated $ApoE^{-/-}$ and $ApoE^{-/-}COMP^{-/-}$ mice (8 weeks old). We evaluated the degree of engraftment after these two exposure doses as approximately 70-93% following bone marrow reconstitution.[11] At 6 weeks post-transplantation, blood from chimeric mice was collected for genotyping and routine blood tests to detect bone marrow reconstitution. Then, the reconstituted mice were fed with Western-type diet (D12108, 40 kcal% fat and 1.25% cholesterol, Research Diets Inc., New Brunswick, NJ, USA) for 16 weeks, and atherosclerotic plaques and calcification were assessed as described above.

Cell Isolation and Culture

Mouse peritoneal macrophages were isolated from thioglycollate-injected mice as described in a previous study.[12] Briefly, each wild type (WT) or $COMP^{-/-}$ mouse was intraperitoneally injected with 5 mL of 2.9% thioglycollate. Four days later, the cells were perfused from the peritoneal cavity and cultured with DMEM (Life Technologies, Grand Island, NY, USA) including 10% fetal bovine serum (FBS) (Life Technologies, Grand Island, NY, USA). Bone marrow cells were isolated and differentiated into bone marrow-derived macrophages (BMDMs) in complete DMEM containing 30% conditioned medium from L929 cells.[13] Primary aortic VSMCs were isolated from the aortas of Sprague-Dawley rats (150-180 g) and cultured with DMEM including 10% FBS as described previously[14], and cells at passage 3-4 were applied for in vitro experiments. Primary bovine aortic endothelial cells (BAECs) were generously donated by Dr. Jing Zhou from Peking University. BAECs were maintained and subcultured in DMEM including 10% FBS as described previously[15].

Aortic Digestion

Aortas, including thoracic (ascending, arch and descending aorta) and abdominal segments, were dissected from $ApoE^{-/-}$ or $ApoE^{-/-}COMP^{-/-}$ mice, and the connective and fat tissues surrounding vessels were removed completely. Aortic tissues were digested into single cells using 1 mL aortic dissociation enzyme solution as described previously.[16] The digested single cell solution was used for flow cytometry or fluorescence activated cell sorting.

Flow Cytometric Analysis and Cell Sorting

Mouse bone marrow cells were labeled using FITC-conjugated anti-mouse CD45, PE-conjugated anti-mouse Gr-1 and APC-conjugated anti-mouse CD11b antibodies to identify myeloid cells. Blood cells were analyzed using FITC anti-CD45 and APC anti-CD11b together with PE-conjugated anti-mouse Ly6C or Ly6G antibodies to identify monocytes or neutrophils, respectively, following the disruption of red blood cells using RBC lysis buffer (Tiangen Biotech Inc., Beijing, China). Co-labeling with PE anti-F4/80 and APC anti-CD11b antibodies was used to distinguish peritoneal macrophages from peritoneal cells isolated from mice without thioglycollate elicitation. For bone marrow-derived macrophages, first, PE anti-F4/80 was applied to identify the differentiated macrophages, and then APC-conjugated anti-mouse CD86 and CD206 antibodies were used to measure the cell-surface protein expression. Macrophages in single-cell suspensions derived from mouse aortas were co-labeled with PE anti-F4/80 and APC anti-CD11b antibodies, and then the cell surface proteins CD86, CD206, and integrin β3 were detected using the corresponding fluorescence-labeled antibodies. To measure Wnt10b in aortic macrophages, cells were permeabilized using BD Cytofix/Cytoperm Fixation/Permeabilization Kit (BD Biosciences, San Diego, CA, USA) following co-labeling with PE anti-F4/80 and APC anti-CD11b antibodies. Permeabilized cells were incubated with rabbit anti-Wnt10b and FITC-labeled anti-rabbit IgG antibodies to measure Wnt10b in aortic macrophages. Generally collected cells (1×10^5/tube) were incubated for 30 min on ice with either the aforementioned antibodies or their respective isotype controls. After the unbound antibodies were washed out, labeled cells were examined using a BD FACS Calibur system (BD Biosciences, San Diego, CA, USA). For analysis, 10,000 cell counts per tube were collected and analyzed using Cell Quest (BD Biosciences, San Diego, CA, USA) or FlowJo (Tree Star Inc., Ashland, OR, USA). For sorting, single-cell suspensions from one atherosclerotic mouse were co-labeled with FITC anti-CD45, PE anti-F4/80 and APC anti-CD11b antibodies, and the triply positive

cells were sorted as lesional macrophages by BD FACS Aria II SORP (BD Biosciences, San Diego, CA, USA) for further RNA isolation and real-time PCR gene detection.

Transmigration Assay

Migration assays were performed using 8.0 μm transwells (BD Biosciences, San Diego, CA, USA) as previously described with minor modifications.[12] Briefly, bovine aortic endothelial cells (BAECs) were grown to confluence on the upper chamber overnight. Mouse mononuclear cells isolated from peripheral blood of WT and $COMP^{-/-}$ mice were stained with CM-DiI dye (Life Technologies, Grand Island, NY, USA) for 20 min. Stained cells were seeded at density of 10^4 per chamber on the upper chamber and coincubated with BAECs and MCP-1 (100 ng/ml) was added to the lower chamber. In 4 hours, cells migrating to the lower chamber were collected and determined using a microplate reader (ThermoFisher Scientific, Grand Island, NY, USA) with excitation at 553 nm and detection at 570 nm.

Gene-expression Microarray

Peritoneal macrophages were isolated from WT and $COMP^{-/-}$ mice injected with thioglycollate, and mRNA was isolated from 2×10^6 cells extracted from 6 mice per sample using Trizol. RNA quantity and quality were measured using NanoDrop ND-1000, whereas RNA integrity was assessed using standard denaturing agarose gel electrophoresis. The microarray experiments were performed by Kang Chen Bio-technology Corp. (Shanghai, China) according to the standard protocol in three independent repeats. A Mouse DNA Array (Roche NimbleGen, Madison, WI, USA) was used to compare gene expression between WT and $COMP^{-/-}$ macrophages.

Briefly, total RNA from each sample was used for labeling and array hybridization using the following steps: 1) Reverse transcription using Invitrogen SuperScript ds-cDNA synthesis kit. 2) ds-cDNA labeling with NimbleGen one-color DNA labeling kit. 3) Array hybridization using the NimbleGen Hybridization System, followed by washing with the NimbleGen wash buffer kit. 4) Array scanning using the Axon GenePix 4000B microarray scanner (Molecular Devices Corporation). Scanned images (TIFFs) were then imported into NimbleScan software (Version 2.5) for grid alignment and expression data analysis. Expression data were normalized using quantile normalization and the Robust Multichip Average (RMA) algorithm included in the NimbleScan software. All gene level files were imported into Agilent GeneSpring GX software (Version 11.5.1) for further analysis. Genes that were expressed at significantly different levels between the two groups were identified through Volcano Plot filtering. Differentially expressed genes were identified through Fold Change filtering (>2.0; <0.5). Pathway Analysis (KEGG) and GO analysis were used to analyze the functions of the differentially expressed genes. Microarray data are available at www.ncbi.nlm.nih.gov/geo/, accession numbers GSE73944.

Aortic Ring Organ Calcification

The aortas were removed from smooth muscle cell specific COMP transgenic (SMC COMP-Tg) mice or littermate wild type C57/BL6 mice. After the adventitia and endothelium were carefully removed, the vessels were cut into 2- to 3-mm rings and placed in a high-phosphate medium (10% FBS DMEM with 3.8 mM inorganic phosphate) or regular DMEM containing 10% FBS at 37°C in 5% CO_2 for 7 consecutive days; the medium was changed every 2 days. Seven days later, the aortic rings were harvested to investigate the level of calcium deposition. The viability of the aortic rings was monitored by a methylthiazoletertrazolium (MTT) assay.[17]

Bioinformatic Correlation Analysis Among Array Data

Gene expression profiles of other macrophage phenotypes including M1, M2, Mox and osteoclast were accessed from www.ncbi.nlm.nih.gov/geo/ (accession numbers GSE32690, GSE66782, GSE35436, GSE46390). The normalized fold changes compared to control untreated macrophages were extracted for further analysis. The fold change profile of COMP KO macrophages relative to WT cells was evaluated for correlation with other macrophage phenotypes via separate Spearman analyses.

Real-time PCR

Total RNA was extracted from mouse peritoneal or bone marrow-derived macrophages, and equal amounts (2 μg) were reverse-transcribed to cDNA. SYBR Green 2× PCR mix (TransGen Biotech, Beijing, China) was used according to the manufacturer's instructions. Primers used in the present study are listed in Online Table I. The PCR program consisted of 94°C for 5 min; 40 cycles of 94°C for 30 s, 56 to 58°C for 30 s, and 72°C for 30 s; and a final extension at 72°C for 5 min. Real-time PCR amplification involved the use of an Mx3000 Multiplex Quantitative PCR System (Stratagene, La Jolla, CA, USA). The mRNA levels were normalized to that of 18s or β-actin.

ROS Production

Reactive Oxygen Species (ROS) production from isolated peritoneal macrophages was measured using the Amplex Red Hydrogen Peroxide/Peroxidase Assay kit (Life Technologies, Grand Island, NY, USA). The assay was performed according to the manufacturer's instructions.

Measurement of Inflammatory Cytokines Secreted by Macrophages

Peritoneal macrophages isolated from WT and COMP KO mice were seeded separately in 60 mm dishes at 1×10^6 cells/dish and cultured for 24 hr. Then, the conditioned medium was collected for analysis using the Mouse Inflammatory Cytokine Cytometric Bead Array (CBA) kit (BD Biosciences, San Diego, CA, USA).

Measurement of Ac-LDL Uptake

Isolated mouse peritoneal macrophages were plated in 60 mm dishes at 1×10^6 cells/dish. DiI-ac-LDL (10 μg/ml) was added and the cells were incubated for 12 hr. Then, macrophages were digested with Accutase and analyzed on an Amnis FlowSight flow cytometer (EMD Millipore, Massachusette, USA) using a 60× objective. Intracellular ac-LDL was analyzed using Amnis IDEAS software (EMD Millipore, Massachusette, USA).

Measurement of Calcium Deposition in VSMCs

VSMCs were grown in 6-well plates and were treated with macrophage-derived conditioned medium for 12 days. After the medium was removed and the cells were washed with phosphate-buffered saline (PBS), VSMCs were treated with 0.6 N HCl overnight at 4°C. After the HCl supernatant was removed, the remaining cell layers were dissolved in 0.1 N NaOH and 0.1% SDS for protein concentration analysis. The calcium content in the HCl supernatant was colorimetrically analyzed using the QuantiChrom Calcium Assay Kit (Zhong Sheng Bio-technology, Beijing, China) and normalized to overall protein concentration.

Western Blotting

Different treated peritoneal macrophages were lysed in RIPA buffer and prepared for extraction of whole-cell protein samples. Then, equal amounts of total protein from macrophages were resolved using 10% SDS-PAGE and transferred onto nitrocellulose membranes. The membranes were incubated with primary antibodies and IRDye-conjugated secondary antibodies. The immunofluorescence signal was detected with an Odyssey infrared imaging system (LICOR Biosciences, Lincoln, NB, USA).

Co-immunoprecipitation

Mouse peritoneal macrophage lysates were incubated with antibodies against COMP or integrin β3 before being immunoprecipitated with protein A/G agarose beads (Santa Cruz Biotechnology). The precipitated proteins were resolved using 10% SDS-PAGE and then immunoblotted with antibodies against integrin β 3 or COMP. Rabbit normal IgG served as a negative control.

Plasmid Transfection

The Amaxa Mouse Macrophage Nucleofector Kit (Lonza Cologne AG, Cologne, Germany) was used to transfer plasmids into mouse peritoneal macrophages. Plasmid transfection in COS-7 cells was performed using jetPEI (Polyplus-transfection SA, Illkrich, France). The transfection procedures followed the manufacturers' instructions.

Adeno-associated Virus Infection in Mice

Mouse integrin β3 full length and β-tail domain (integrin β3 aa 629-717) were cloned into adeno-associated virus serotype 2 (AAV2) vector pAV-FH (Vigene Inc., Shandong, China), and AAV2 vector pAV-C-GFP was applied as negative control. Then recombinant AAV2 plasmids were co-transfected with Ad-helper vector and pAAV-rep/cap vector into HEK293T cells for 72 hours. Supernatant was collected for further purification by PEG8000 precipitation. Purified AAV virus was applied for *in vivo* experiments.

Four-month-old male $ApoE^{-/-}$ or 7-month-old $ApoE^{-/-}COMP^{-/-}$ mice were injected with AAV2-GFP, AAV2-integrin β3 or AAV2-β-tail domain virus as a titer of 1×10^{11} v.g./ml via tail vein with 200 μl virus per mouse. Western-type diet (D12108, 40 kcal% fat and 1.25% cholesterol, Research Diets Inc., New Brunswick, NJ, USA) was provided from the first day of injection and maintained for 4 weeks. Peritoneal macrophages were firstly isolated for validating the virus infection efficiency via measuring the percentage of GFP^+ cells by flow cytometry and the expression of integrin β3 and β-tail domain by western blotting and real-time PCR. Then atherosclerotic plaques and calcification and lesional macrophages were assessed as described above.

Lentivirus Package and Infection

Rat COMP shRNA lentivirus were packaged as described previously[18] and the package system was generously sent by Dr. Guang Hu from National Institute of Environment Health Sciences (Research Triangle Park, NC, USA). Briefly, oligo DNA coding COMP shRNA was designed via DSIR (http://biodev.extra.cea.fr/DSIR/DSIR.html) and shRNA retriever (http://cancan.cshl.edu/RNAi_central/RNAi.cgi?type=shRNA) online tools. COMP shRNA oligo was synthesized by Sunbio company (Beijing, China) and amplified into two-strand DNA fragment by PCR. The DNA fragment was subcloned into pHAGE-Mir-Phes vector, and pHAGE-Mir-EF vector was applied as negative control. Then pHAGE vectors were co-transfected with virus package vectors

including PM2, Rev, Tat and VSV-G into HEK293T cells. Following 48-hour culture, supernatant was collected as virus stock for further infection in rat primary VSMCs.

Mammalian Two-Hybrid Assay

Fragments encoding the four functional domains of mouse COMP (the N terminus (aa 20-83), EGF repeats (aa 84-261), type III repeats (aa 266-520), and the C terminus (aa 521-755)) were amplified by PCR and subcloned into pACT.[19] The cDNA inserts encoding the full-length mouse integrin β3 and various domains including aa 1-461 (A-, Hybrid and PSI domains), aa 462-628 (EGF repeats), aa 629-717 (β -tail domain), and aa 718-787 (TM and cytoplasmic domains) were subcloned in-frame into the pBIND vector to generate the indicated plasmids. COS-7 cells were cotransfected with the target and bait constructs together with the luciferase reporter plasmid pG5luc at a ratio of 1:1:1. After 48 h, the transfected cells were harvested, and cell lysates were used for luciferase activity assays with the Dual-Luciferase Reporter Assay System (Promega, Madison, WI, USA).

Statistical Analysis

Values are expressed as the mean ± standard error of the mean (SEM). Treatment group values were compared with their controls using GraphPad Prism 6.0 (GraphPad Software, San Diego, California, USA). Comparisons of gene expression, cytokine release and ROS production between WT and COMP-/- macrophages, as well as the expression levels of genes in lesional macrophages between $ApoE^{-/-}$ and $ApoE^{-/-}COMP^{-/-}$ mice, were analyzed using the unpaired two-tailed Student's t test. The statistical analysis of the mammalian two-hybrid assay involved one-way ANOVA followed by the Student-Newman-Keuls test for post hoc comparison. Two-way ANOVA followed by the Bonferroni test was applied for comparisons of calcium deposition in VSMCs cultured with macrophages conditioned medium, and gene expression in WT and $COMP^{-/-}$ macrophages following integrin β3 overexpression. Data of atherosclerotic lesion, calcification and plaque compositions are non-normalized distribution. Comparisons of atherosclerotic lesion, calcification and plaque compositions were analyzed by nonparametric tests, which were Mann-Whitney test for assessment between $ApoE^{-/-}$ and $ApoE^{-/-}COMP^{-/-}$ mice and Kruskal-Wallis test followed by Dunn's test for bone marrow transplantation experiments. In all cases, statistical significance was concluded where the two-tailed probability was less than 0.05.

Reference

1. Svensson L, Aszodi A, Heinegard D, Hunziker EB, Reinholt FP, Fassler R, Oldberg A. Cartilage oligomeric matrix protein-deficient mice have normal skeletal development. *Mol Cell Biol*. 2002;22:4366-4371
2. Callegari A, Coons ML, Ricks JL, Yang HL, Gross TS, Huber P, Rosenfeld ME, Scatena M. Bone marrow- or vessel wall-derived osteoprotegerin is sufficient to reduce atherosclerotic lesion size and vascular calcification. *Arterioscler Thromb Vasc Biol*. 2013;33:2491-2500
3. Maganto-Garcia E, Tarrio M, Lichtman AH. Mouse models of atherosclerosis. *Curr Protoc Immunol*. 2012;Chapter 15:Unit 15 24 11-23
4. Tangirala RK, Rubin EM, Palinski W. Quantitation of atherosclerosis in murine models: Correlation between lesions in the aortic origin and in the entire aorta, and differences in the extent of lesions between sexes in ldl receptor-deficient and apolipoprotein e-deficient mice. *J Lipid Res*. 1995;36:2320-2328

5. Rattazzi M, Bennett BJ, Bea F, Kirk EA, Ricks JL, Speer M, Schwartz SM, Giachelli CM, Rosenfeld ME. Calcification of advanced atherosclerotic lesions in the innominate arteries of apoe-deficient mice: Potential role of chondrocyte-like cells. *Arterioscler Thromb Vasc Biol*. 2005;25:1420-1425
6. Nguyen N, Naik V, Speer MY. Diabetes mellitus accelerates cartilaginous metaplasia and calcification in atherosclerotic vessels of ldlr mutant mice. *Cardiovasc Pathol*. 2013;22:167-175
7. Rosenfeld ME, Polinsky P, Virmani R, Kauser K, Rubanyi G, Schwartz SM. Advanced atherosclerotic lesions in the innominate artery of the apoe knockout mouse. *Arterioscler Thromb Vasc Biol*. 2000;20:2587-2592
8. Seimon TA, Wang Y, Han S, Senokuchi T, Schrijvers DM, Kuriakose G, Tall AR, Tabas IA. Macrophage deficiency of p38alpha mapk promotes apoptosis and plaque necrosis in advanced atherosclerotic lesions in mice. *J Clin Invest*. 2009;119:886-898
9. Duran-Struuck R, Dysko RC. Principles of bone marrow transplantation (bmt): Providing optimal veterinary and husbandry care to irradiated mice in bmt studies. *J Am Assoc Lab Anim Sci*. 2009;48:11-22
10. Forristal CE, Winkler IG, Nowlan B, Barbier V, Walkinshaw G, Levesque JP. Pharmacologic stabilization of hif-1alpha increases hematopoietic stem cell quiescence in vivo and accelerates blood recovery after severe irradiation. *Blood*. 2013;121:759-769
11. Liang Y, Fu Y, Qi R, Wang M, Yang N, He L, Yu F, Zhang J, Yun CH, Wang X, Liu J, Kong W. Cartilage oligomeric matrix protein is a natural inhibitor of thrombin. *Blood*. 2015;126:905-914
12. Fu Y, Moore XL, Lee MK, Fernandez-Rojo MA, Parat MO, Parton RG, Meikle PJ, Sviridov D, Chin-Dusting JP. Caveolin-1 plays a critical role in the differentiation of monocytes into macrophages. *Arterioscler Thromb Vasc Biol*. 2012;32:e117-125
13. Weischenfeldt J, Porse B. Bone marrow-derived macrophages (bmm): Isolation and applications. *CSH Protoc*. 2008;2008:pdb prot5080
14. Ross R. The smooth muscle cell. Ii. Growth of smooth muscle in culture and formation of elastic fibers. *J Cell Biol*. 1971;50:172-186
15. Fu Y, Hou Y, Fu C, Gu M, Li C, Kong W, Wang X, Shyy JY, Zhu Y. A novel mechanism of gamma/delta t-lymphocyte and endothelial activation by shear stress: The role of ecto-atp synthase beta chain. *Circ Res*. 2011;108:410-417
16. Butcher M, Herre M, Ley K, Galkina E. Flow cytometry analysis of immune cells within murine aortas. *Journal of Visualized Experiments Jove*. 2011
17. Gao C, Fu Y, Li Y, Zhang X, Zhang L, Yu F, Xu SS, Xu Q, Zhu Y, Guan Y, Wang X, Kong W. Microsomal prostaglandin e synthase-1-derived pge2 inhibits vascular smooth muscle cell calcification. *Arterioscler Thromb Vasc Biol*. 2016;36:108-121
18. Stegmeier F, Hu G, Rickles RJ, Hannon GJ, Elledge SJ. A lentiviral microrna-based system for single-copy polymerase ii-regulated rna interference in mammalian cells. *Proc Natl Acad Sci U S A*. 2005;102:13212-13217
19. Huang Y, Xia J, Zheng J, Geng B, Liu P, Yu F, Liu B, Zhang H, Xu M, Ye P, Zhu Y, Xu Q, Wang X, Kong W. Deficiency of cartilage oligomeric matrix protein causes dilated cardiomyopathy. *Basic Res Cardiol*. 2013;108:374

Online Figure Legends

Online Figure I. COMP deficiency accelerates atherosclerotic lesions. (A) Representative images and quantification of aortic enface Oil Red O (ORO) staining in 12-month-old ApoE$^{-/-}$ and ApoE$^{-/-}$COMP$^{-/-}$ mice fed with chow diet. * P<0.05. **(B)** Representative ORO staining on cross sections of aortic root, aortic arch or innominate artery from ApoE$^{-/-}$ and ApoE$^{-/-}$COMP$^{-/-}$ mice. Scale bar = 200 μm (Aortic Root) and 100 μm (Aortic Arch and Innominate Artery). **(C)** Quantification of ORO staining areas in different parts of artery. *P<0.05

Online Figure II. COMP deficiency enhanced atherosclerotic lesions. (A) Representative von Kossa staining on cross sections of aortic root or aortic arch from 12-month-old ApoE$^{-/-}$ and ApoE$^{-/-}$COMP$^{-/-}$ mice fed with chow diet. Scale bar = 200 μm (Aortic Root) and 100 μm (Aortic Arch). **(B)** Quantification of stained calcification areas in aortic root or arch. * P<0.05

Online Figure III. (A) Western blot of COMP in vascular endothelial cells (EC), smooth muscle cells (VSMC) and adventitial fibroblasts (AF). (B) Western blot of COMP in mouse lymphocytes and macrophages.

Online Figure IV. Blood genotypes of chimeric mice created by bone marrow transplantation.

Online Figure V. Both bone marrow- and non bone marrow-derived COMP is involved in atherogenesis. Representative images **(A)** and quantification **(B)** of ORO staining on cross sections of innominate arteries from chimeric mice created by bone marrow cross-transplantation between ApoE$^{-/-}$ and ApoE$^{-/-}$COMP$^{-/-}$ mice that were fed a Western-type diet for 16 weeks. Scale bar=200 μm, * P<0.05

Online Figure VI. VSMC-derived COMP does not play a critical role in atherosclerotic calcification. (A) DNA construct used for generation of SMC specific transgenic mice. (**B)** Four independent COMP-Tg lines were analyzed (L.2, L.3, L.4 and L.5). Western blot of COMP in WT and COMP-Tg aortas, and three aortas were pooled as one sample. **(C)** Western blot analysis of COMP in different tissues from the L.3 transgenic line. **(D)** Calcium deposition of aortic rings from 12-week old WT and SMC COMP-tg mice. n=5, *P<0.05. **(E)** Representative images of Movat staining on cross sections of innominate artery from 6-month-old ApoE$^{-/-}$ and SMC COMP-tg ApoE$^{-/-}$ mice fed with Western-type diet for 12 weeks. Black arrows indicate necrotic core, while red arrows indicate chondrocyte-like cells. Scale bar=100 μm (100×) and 20 μm (400×). Statistical analysis in the plaque area **(F)** and the percentages of cartilaginous metaplasia area **(G)**, plaque containing chondrocyte-like cells **(H)** and necrotic core area **(I)** in atherosclerotic lesion.

Online Figure VII. Bone marrow cells, blood cells and peritoneal cells isolated from individual WT and COMP$^{-/-}$ mice. The percentages of myeloid cells **(A)**, ly6C^{low} monocytes **(B)**, ly6C^{high} monocytes **(C)**, neutrophils **(D)** and peritoneal macrophages **(E)** were analyzed via flow cytometry. n=6, *P<0.05. **(F)** The transmigration of mononuclear cells from the peripheral blood of WT and COMP$^{-/-}$ mice via BAECs monolayer. n=5, * P<0.05.

Online Figure VIII. Microarray analysis of GO pathways including biological process, cellular component

and metabolic function and KEGG pathways upregulated **(A)** or downregulated **(B)** by COMP deficiency.

Online Figure IX. Heatmap of representative genes related to inflammation, endocytosis, ROS production and osteogenesis in comparable microarray between WT and $COMP^{-/-}$ peritoneal macrophages.

Online Figure X. Isolated bone marrow cells from WT and $COMP^{-/-}$ mice were differentiated into macrophage by L929 cell conditional medium for 7 days. Bone marrow-derived macrophages (BMDMs) were activated by IFNγ (10 ng/mL) for 24 hours and considered M1 macrophages. **(A)** IL-12 and iNOS were measured and quantified by real-time PCR. **(B)** Statistical result of the mean fluorescent intensity (MFI) of CD86 detected by flow cytometry in IFNγ–induced BMDMs. BMDMs were stimulated by IL-4 (10 ng/mL) for 24 hours and considered M2 macrophages. **(C)** Relative mRNA levels of Ym-1 and Arg 1 quantified via real-time PCR. **(D)** Statistical result of CD206 MFI in IL-4-stimulated BMDMs measured by flow cytometry. **(E)** Measurement of H_2O_2 produced in conditioned medium from IFNγ–treated BMDMs. **(F)** Relative mRNA of Wnt10b in IFNγ-elicited BMDMs. n=6, **P*<0.05

Online Figure XI. Integrin β3 mediates the phenotypic shift of macrophages induced by COMP deficiency. (A) Relative mRNA quantification of integrin β1 and integrin β3 in WT and $COMP^{-/-}$ peritoneal macrophages by real-time PCR. **(B)** Western blot and quantification of integrin β1 and integrin β3 in WT and $COMP^{-/-}$ peritoneal macrophages. Three independent experiments were performed in duplicate. n=3, **P*<0.05. **(C)** Flow cytometric analysis of integrin β3 in lesional macrophages from $ApoE^{-/-}$ and $ApoE^{-/-}COMP^{-/-}$ mice. Bar graph indicates the MFI statistical result. n=6, **P*<0.05. WT and $COMP^{-/-}$ peritoneal macrophages were transfected with pcDNA3.1 or pcDNA3.1-integrin β3 plasmids, respectively. **(D-I)** The relative mRNA levels of TLR4, IL-6, iNOS, p47phox, LOX-1 and Wnt10b were measured using real-time PCR. n=3, **P*<0.05

Online Figure XII. (A) Flow cytometric analysis of GFP expression in peritoneal macrophages from $ApoE^{-/-}$ mice with (blue curve) or without (red curve) AAV2-GFP infection. Real-time PCR **(B)** and western blot **(C)** of integrin β3 in peritoneal macrophages from $ApoE^{-/-}COMP^{-/-}$ mice infected with AAV2-GFP or AAV2-integrin β3. n=3, **P*<0.05. **(D)** Quantification of plaque area on cross sections of innominate arteries from $ApoE^{-/-}COMP^{-/-}$ mice infected with AAV2-GFP or AAV2-intergin β3 followed by 4-week Western-type diet feeding. **P*<0.05

Online Figure XIII. Integrin β3 is not involved in COMP deficiency-induced VSMC dedifferentiation. Rat aortic VSMCs were infected with control shRNA or COMP shRNA lentivirus (100 MOI). Four days later, integrin β3 was measured by real-time PCR **(A)** and western blot **(B)**. Three independent experiments were performed in duplicate. n=3. **(C-E)** Rat aortic VSMCs were infected with control shRNA or COMP shRNA lentivirus and AAV2-GFP or AAV2-integrin β3 for 4 days. The relative mRNA levels of sm22, SMA and calponin were measured using real-time PCR. Three independent experiments were performed in duplicate. n=3

Online Figure XIV. (A) Peritoneal macrophages isolated from WT mice injected with thioglycollate were transfected with pcDNA3.1 or pcDNA3.1-integrin β3 DN plasmids. Twenty-four hours later, integrin β3 was detected in protein fractions immunoprecipitated from the lysis of transfected cells via western blot. Rabbit

IgG was used as a negative control for IP. Input fractions isolated prior to precipitation were detected for loading controls. **(B)** Relative mRNA of β-tail domain was measured by real-time PCR in peritoneal macrophages isolated from ApoE$^{-/-}$ mice infected with AAV2-GFP or AAV2-β-tail domain. n=3, **P*<0.05. **(C)** Western blot of integrin β3 in peritoneal macrophages isolated from ApoE$^{-/-}$ mice infected with AAV2-GFP or AAV2-β-tail domain. Cells from three mice were pooled as one sample. **(D)** Quantification of plaque area on cross sections of innominate arteries from ApoE$^{-/-}$ mice infected with AAV2-GFP or AAV2-β-tail domain followed by 4-week Western-type diet feeding. **P*<0.05

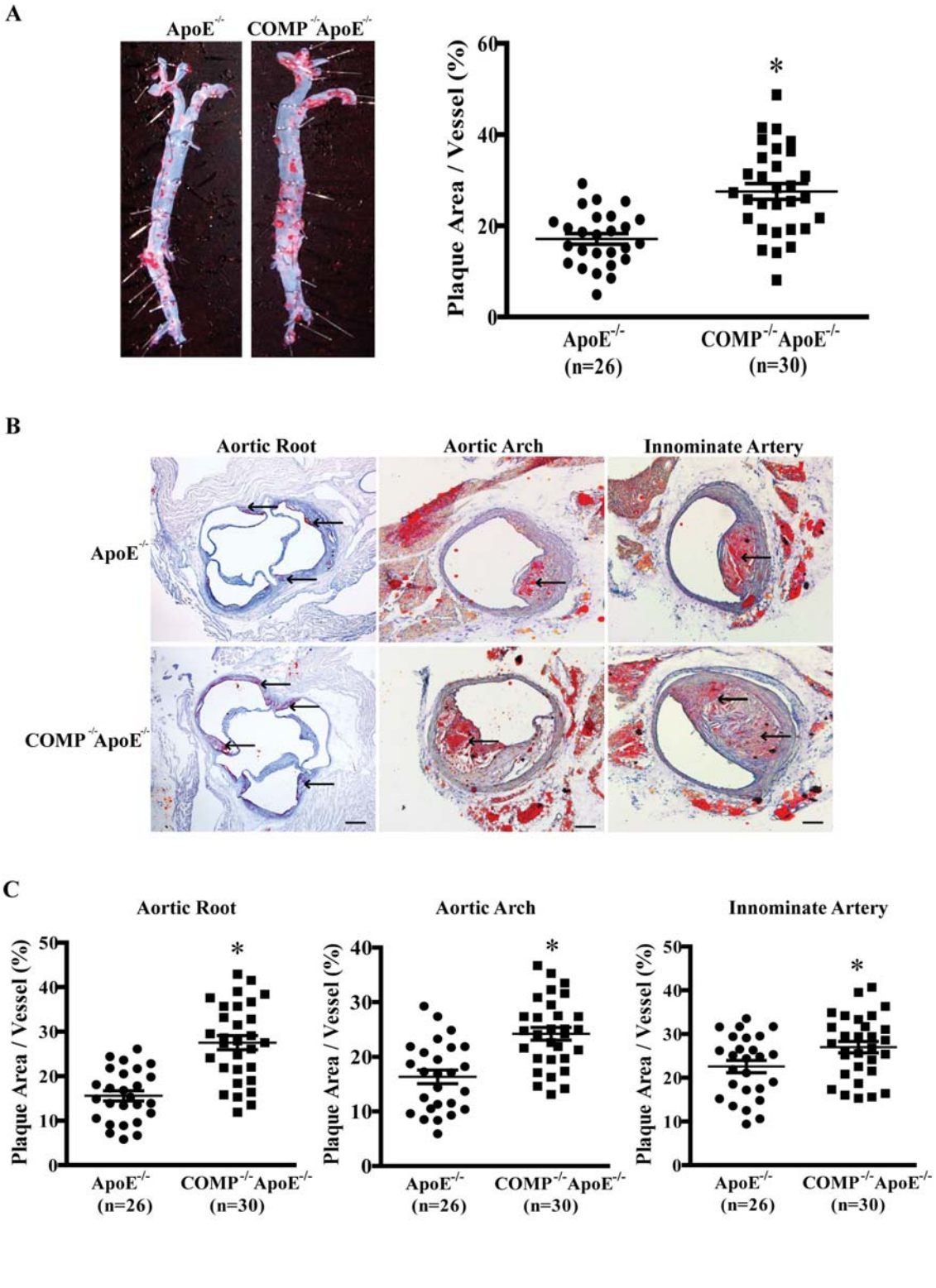

Online Figure I

A

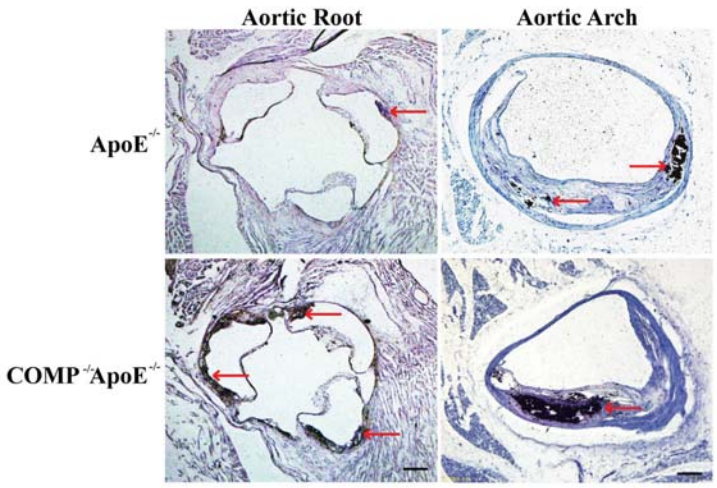

B

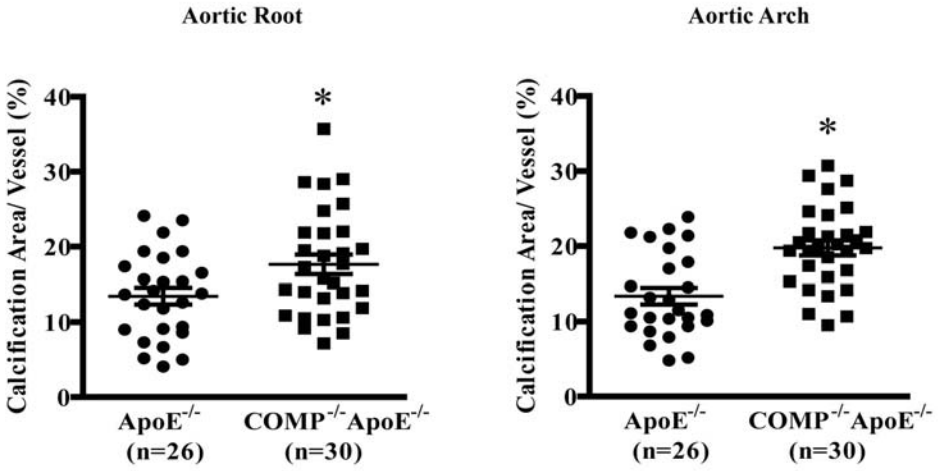

Online Figure II

A

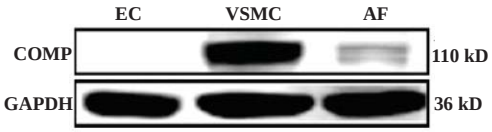

B

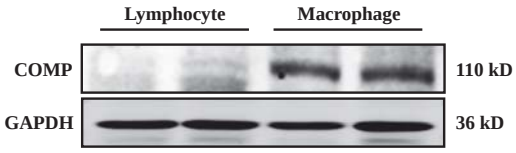

Online Figure III

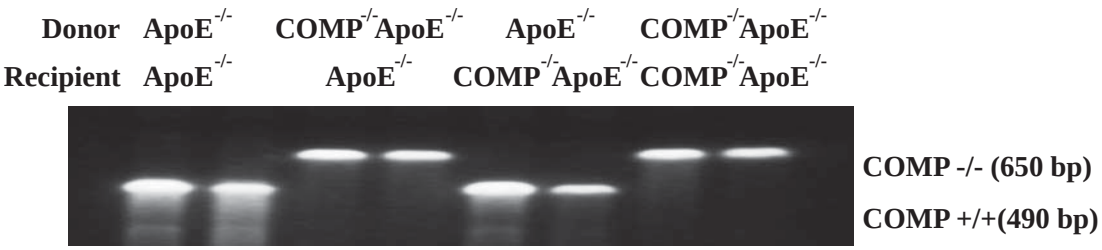

Online Figure IV

A

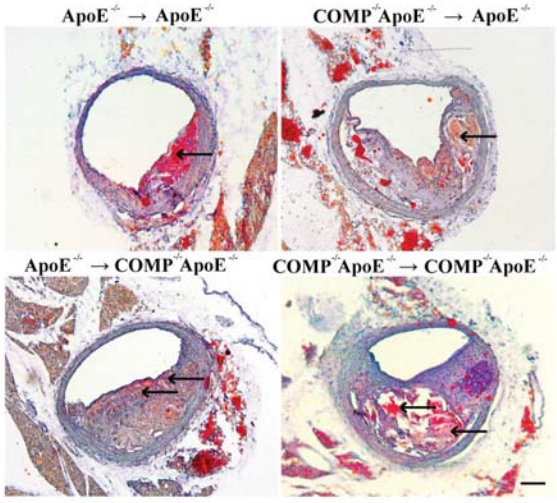

B

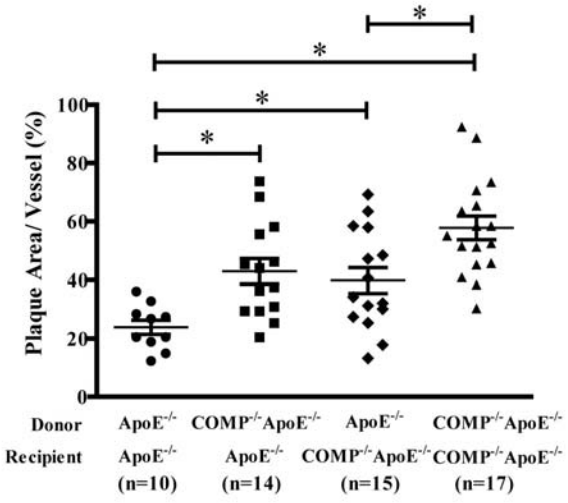

Online Figure V

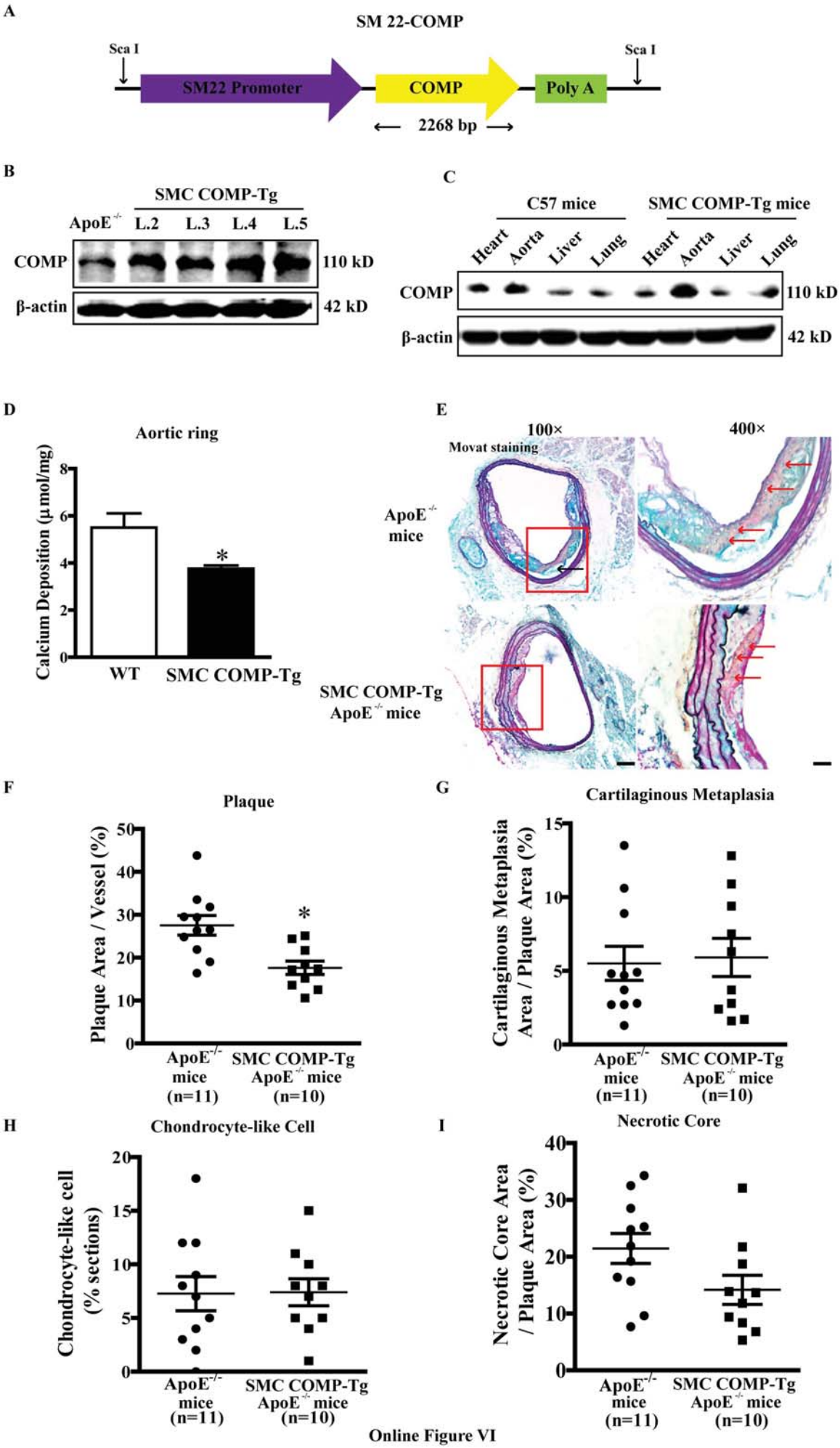

Online Figure VI

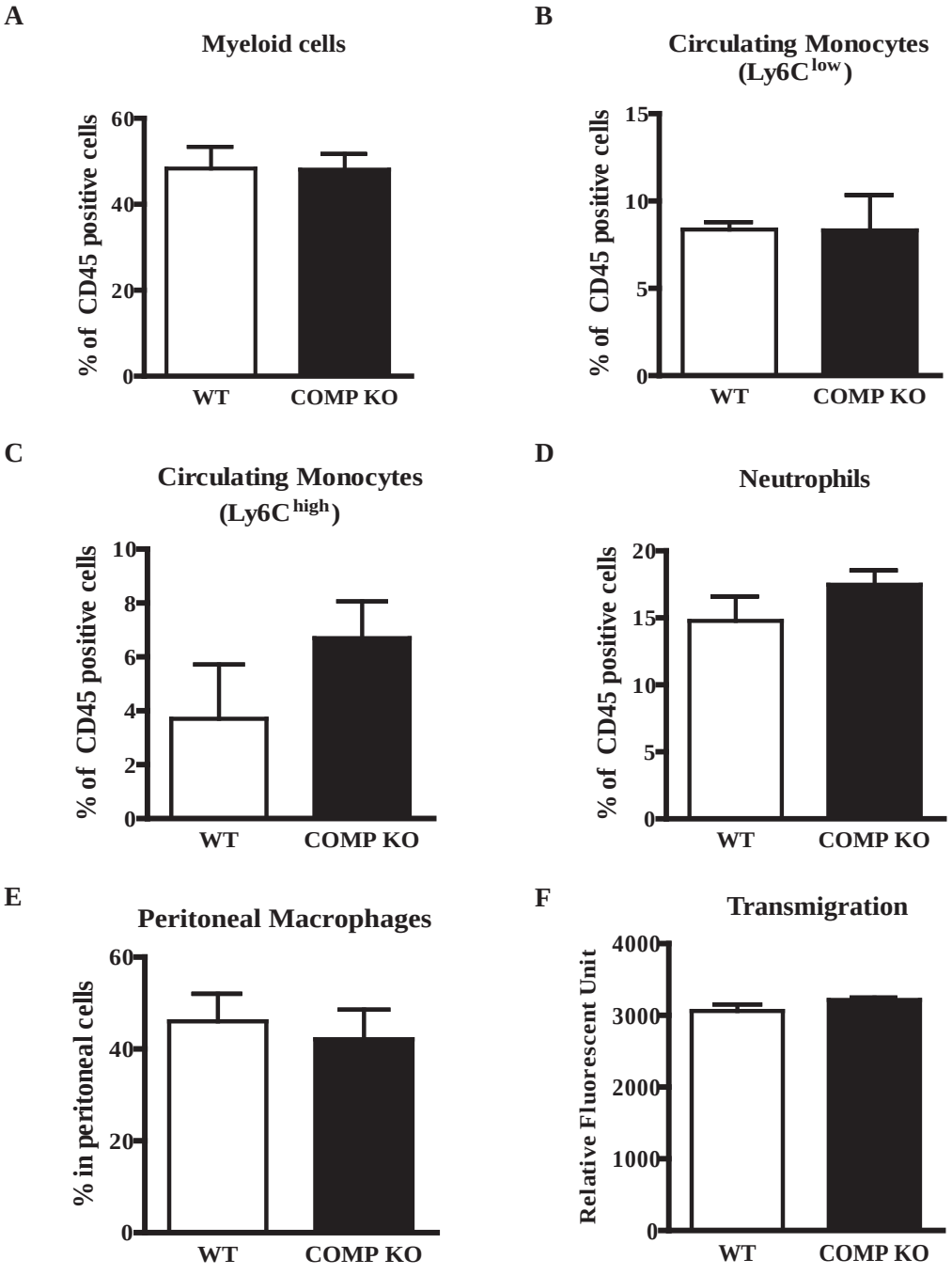

Online Figure VII

A Upregulation

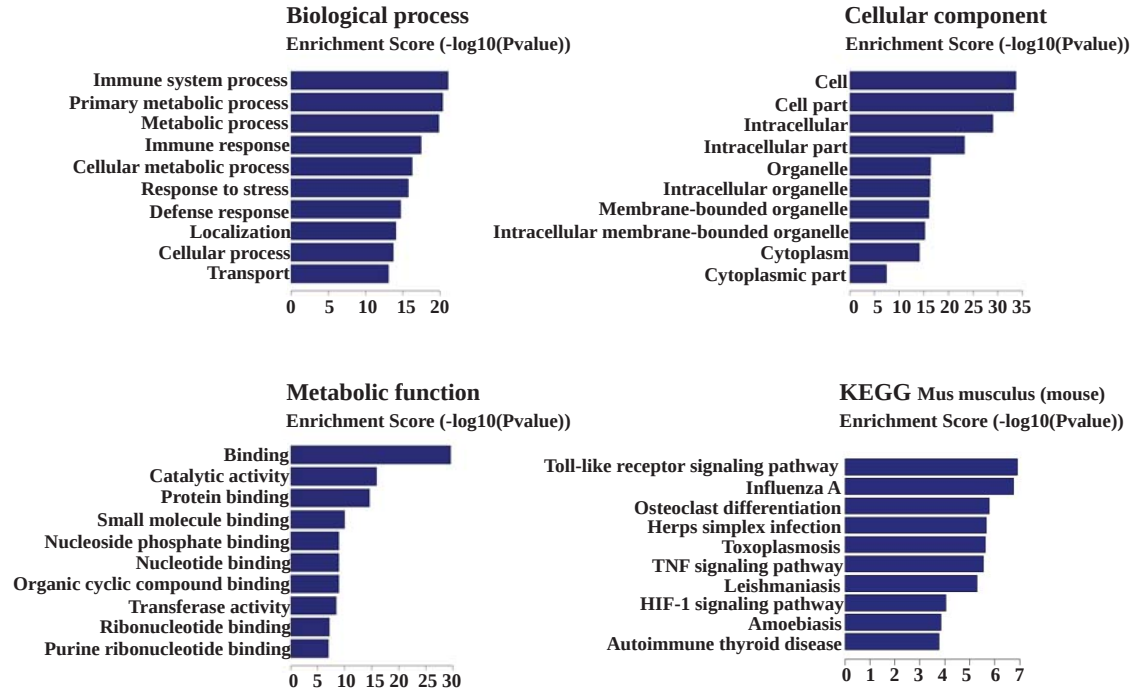

B Downregulation

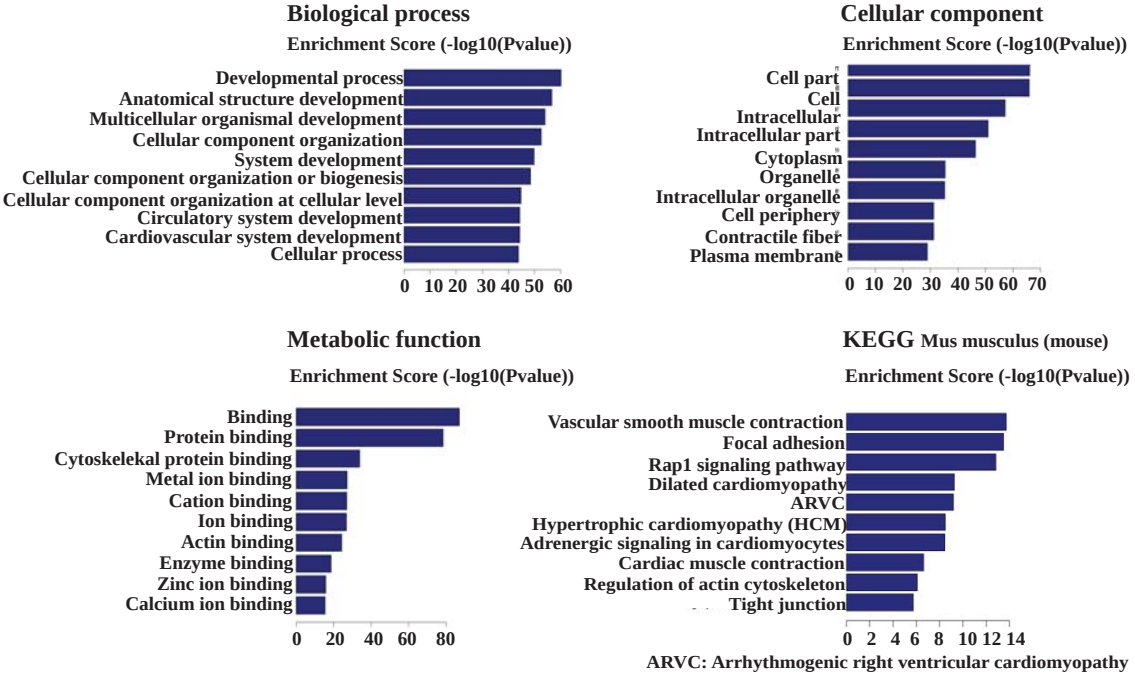

ARVC: Arrhythmogenic right ventricular cardiomyopathy

Online Figure VIII

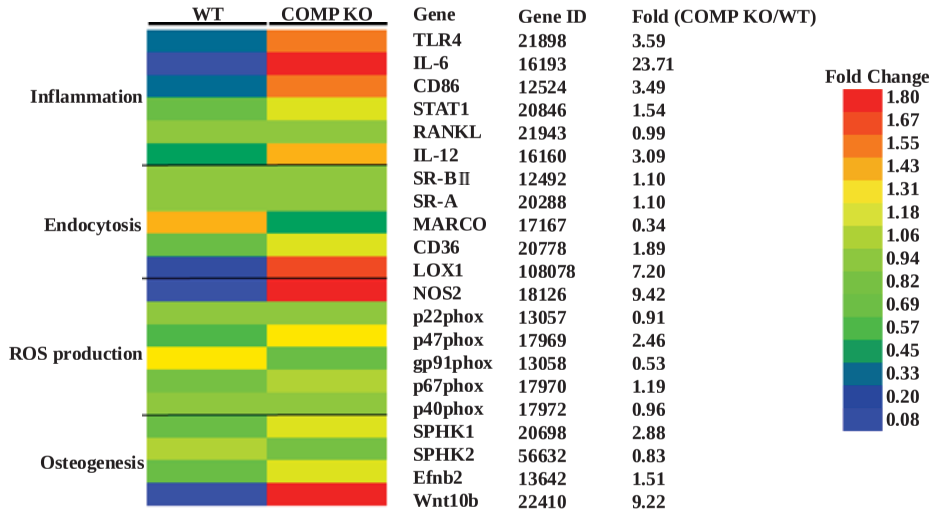

Oline Figure IX

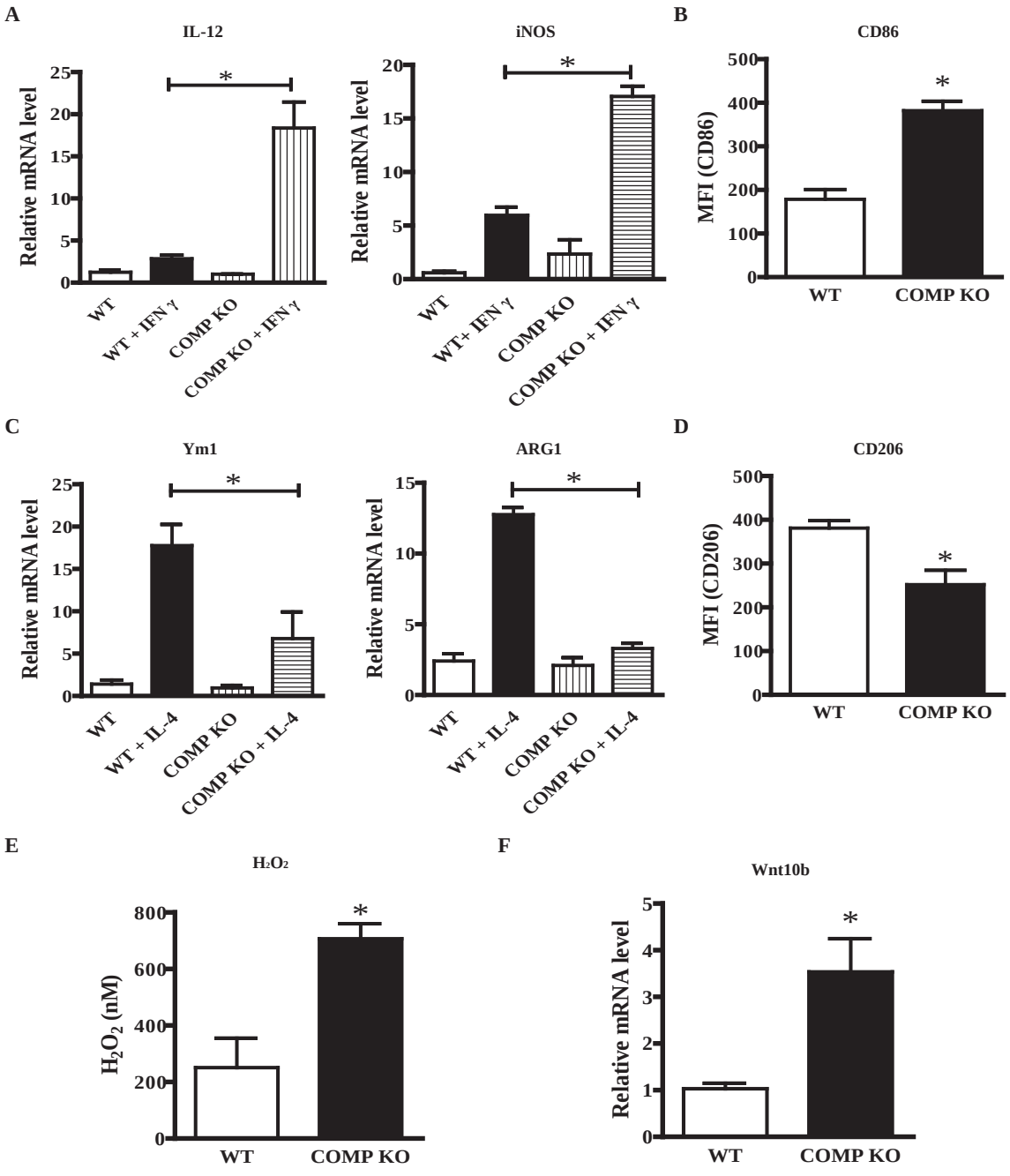

Online Figure X

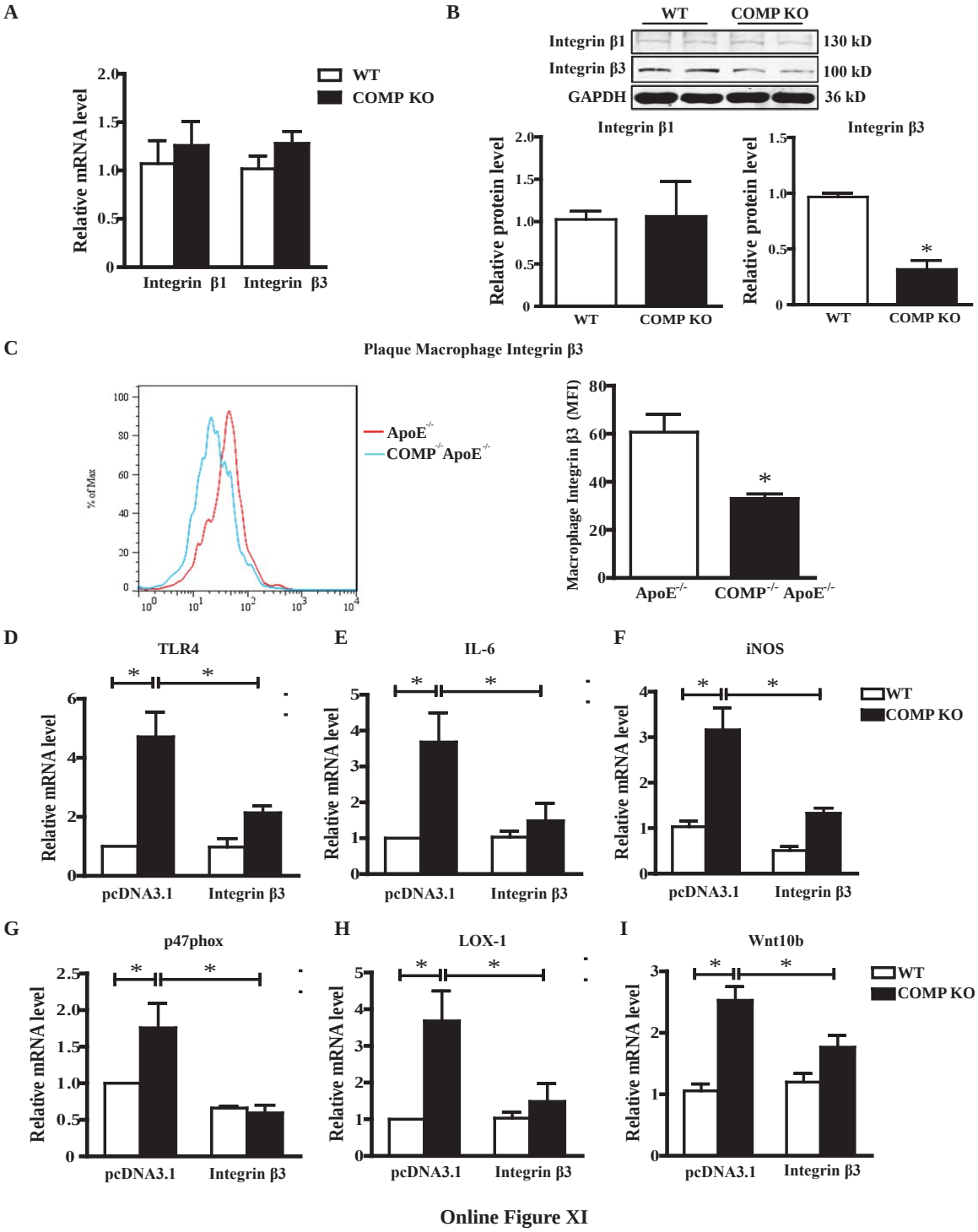

Online Figure XI

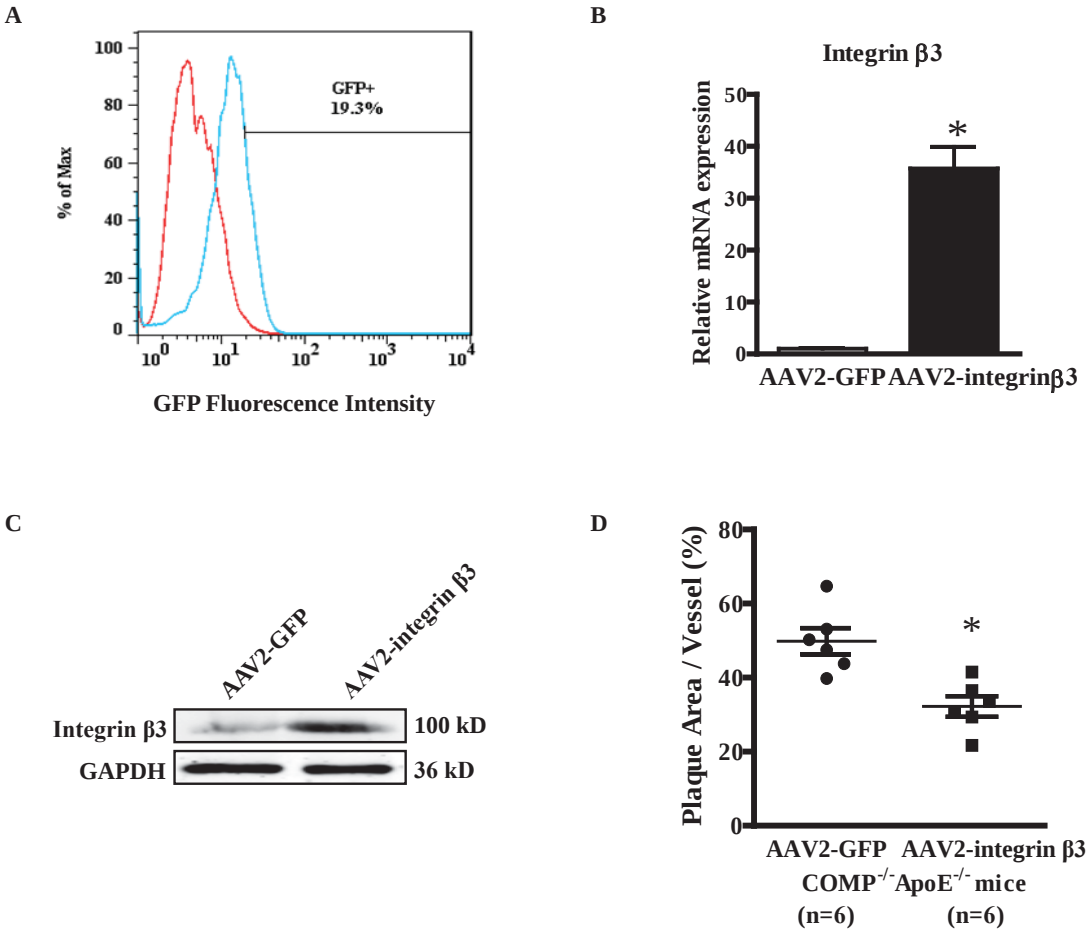

Online Figure XII

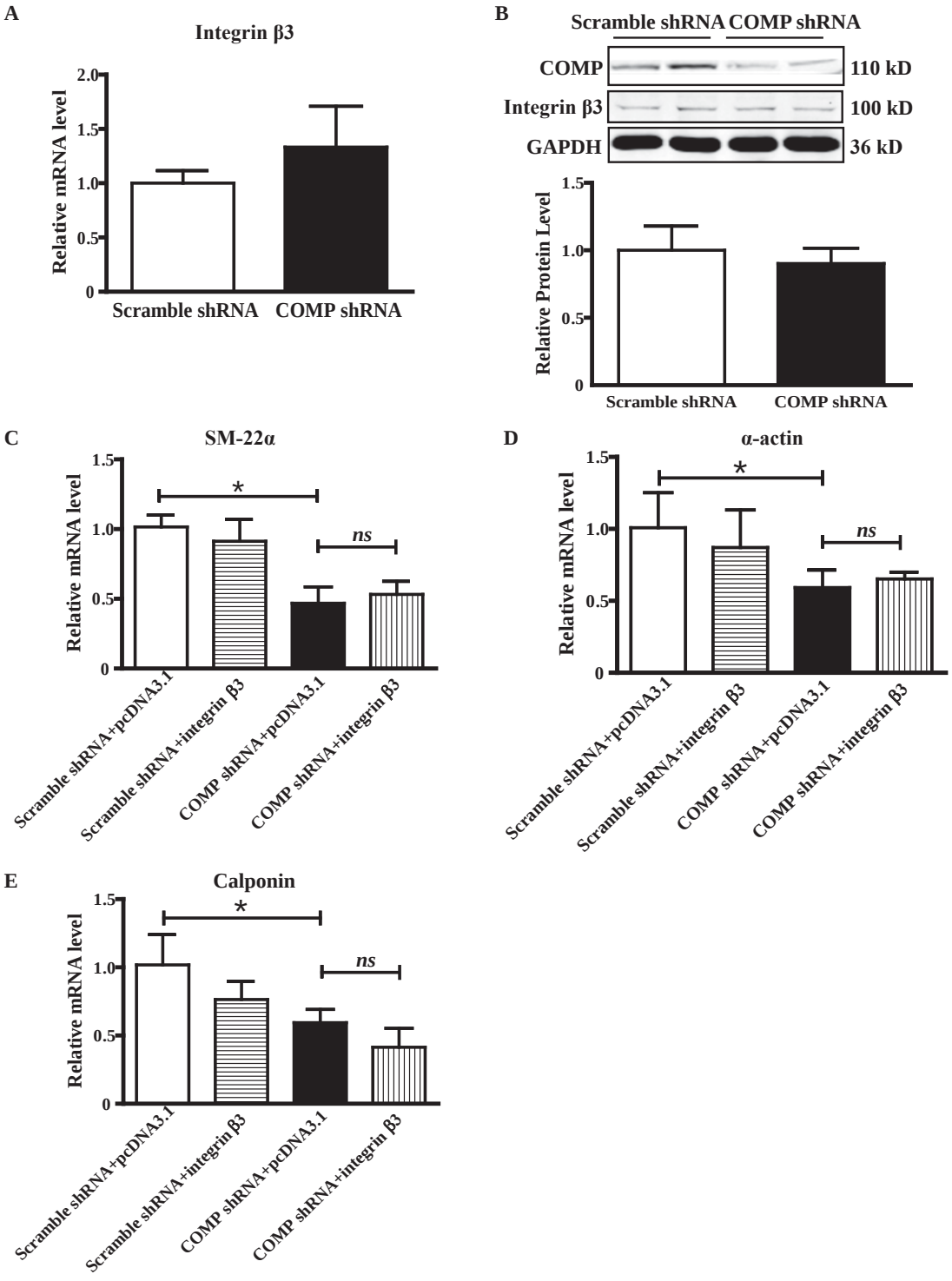

Online Figure XIII

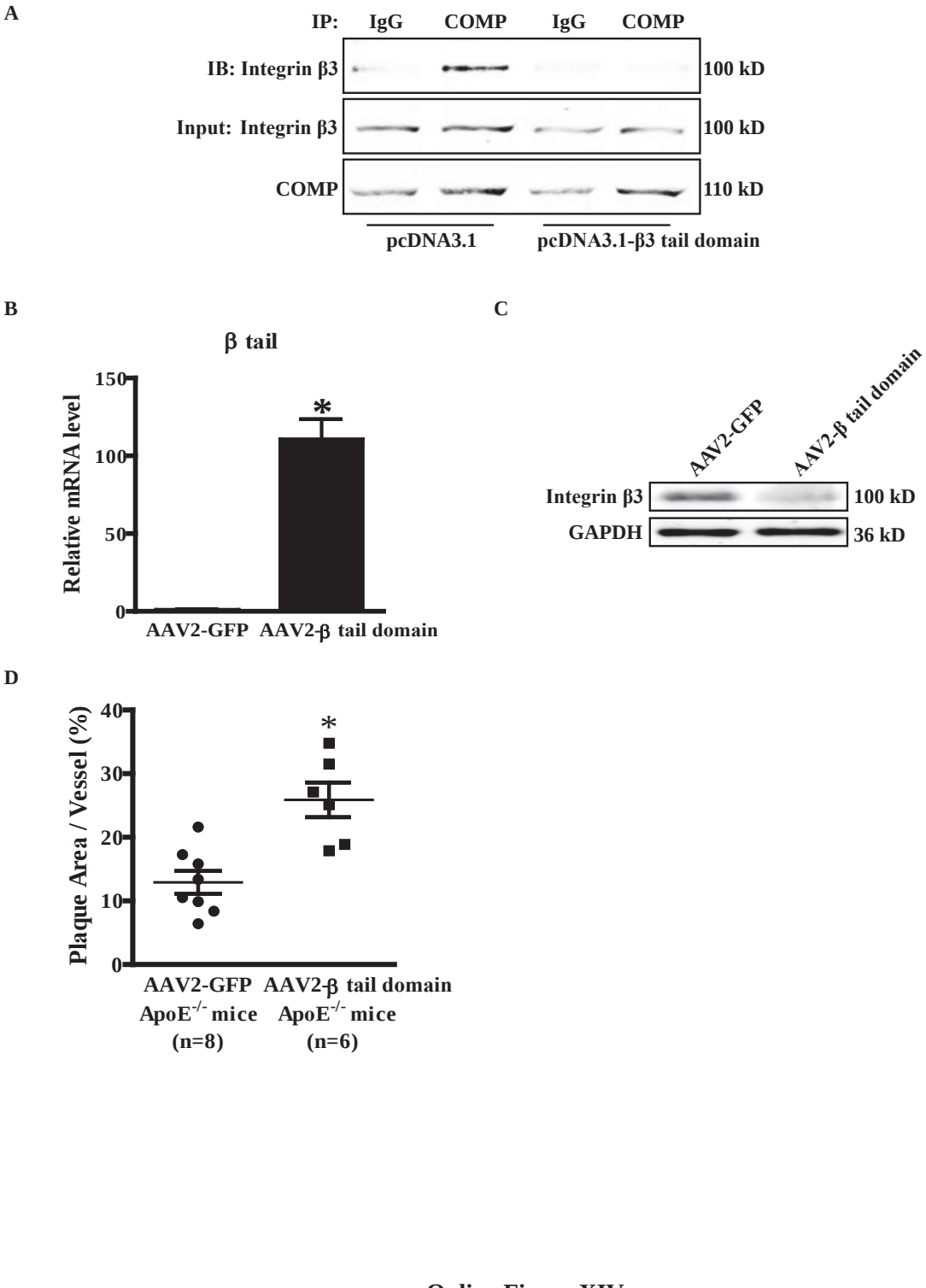

Online Figure XIV

Online Table I. RT-PCR Primers.

	Forward primer (5'-3')	Reverse primer (5'-3')
Mouse TLR4	ACACTTTATTCAGAGCCGTTG	TTTTCCATCCAATAGGGCAT
Mouse IL-6	TCCAGGAGCCCAGCTATGAC	AGATGCCGTCGAGGATGTACC
Mouse IL-12	CCAGGTGTCTTAGCCAGTCC	GCAGTGCAGGAATAATGTTTCA
Mouse iNOS	CTTTGCCACGGACGAGAC	TCATTGTACTCTGAGGGCTGAC
Mouse p47phox	CCTTCAGACCTATCGGGCCAT	CTCGCTCTTCTCCACAACGTCCA
Mouse LOX-1	CAAGATGAAGCCTGCGAAT	TACCTGGCGTAATTGTGTCC
Mouse Wnt10b	CGCTGCCACTGTCGTTTCC	TTCTCCTCCTCGTCGTGCCTA
Mouse Sphk1	CTTCAAGGCGTGACCTAGTT	CTCTATCTTCGCATCGCTTCT
Mouse Integrin β1	CAACCACAACAGCTGCTTCTAA	TCAGCCCTCTTGAATTTTAATGT
Mouse Integrin β3	TGCCACCTGCCTCAACAACGA	CCCACACTCAAAAGTCCCGTTC
Mouse Arg 1	CATTGTCCTTAAGCCGTTCC	CAGCCAACATCCCCACAT
Mouse Ym 1	AAGAACACTGAGCTAAAAACTCTCCT	GAGACCATGGCACTGAACG
Mouse β tail domain	TGCCCAGATGCCTGCTCCTTT	ATCAGGACCCTTGGGACACTC
Mouse 18s	TTGACGGAAGGGCACCACCAG	GCACCACCACCCACGGAATCG
Mouse β-actin	CAAAGACCTGTACGCCAACAC	TCATAGTCCGCCTAGAAG
Rat α-actin	ACTCTGGAGATGGCGTGACTC	GCGTTCATTCCCGATGGT
Rat SM-22α	TCCTTCCAGCCCACAAACGAC	GGGCCACACTGCATTACAATC
Rat calponin	CCAGCATGTCTTCCGCACACT	CCATGAAGTTGCTCCCGATG
Rat β-actin	GAGACCTTCAACACCCCAGCC	TCGGGGCATCGG AACCGCTCA

Online Table II. Body weight, blood pressure, serum lipid profile, and serum biochemical measurements of 12-month-old ApoE$^{-/-}$ and COMP$^{-/-}$ApoE$^{-/-}$ mice fed with chow diet.

	ApoE$^{-/-}$ mice (n=26)	COMP$^{-/-}$ApoE$^{-/-}$ mice (n=30)
Body weight (g)	28.873±0.734	31.088±0.701
Blood pressure (mmHg)	105.912±2.109	110.254±3.775
Complete blood count:		
WBC ($\times 10^9$/L)	4.883±0.583	4.867±0.329
RBC ($\times 10^{12}$/L)	8.138±0.633	8.787±0.318
PLT ($\times 10^9$/L)	283.200±45.157	211.400±10.977
GRN ($\times 10^9$/L)	1.633±0.244	1.450±0.373
LYM ($\times 10^9$/L)	1.567±0.263	1.450±0.315
Serum lipid profile:		
TC (mg/dl)	194.123±46.813	219.020±41.461
TG (mg/dl)	201.177±29.299	186.151±21.586
HDL (mg/dl)	31.033±4.135	31.919±1.201
LDL (mg/dl)	157.137±22.614	169.463±28.160
Serum biochemical measurements:		
Pi (mM)	1.832±0.184	1.716±0.086
Ca (mM)	1.784±0.115	1.828±0.184
BUN (mM)	2.332±0.314	2.425±0.251
Cre (μM)	24.762±1.893	23.832±1.275

WBC, white blood cells; **RBC**, red blood cells; **PLT,** platelet; **GRN**, neutrophilic granulocyte; **LYM**, lymphocyte; **TC**, total cholesterol; **TG**, triglycerides; **HDL**, high density lipoprotein; **LDL**, low density lipoprotein; **Pi**, phosophorus; **Ca**, calcium; **BUN**, blood urea nitrogen; **Cre**, creatinine.

Data were presented as Mean±SEM.

Online Table III. Body weight, blood pressure, plasma COMP level, serum lipid profile, and serum biochemical measurements of chimeric mice fed with Western-type diet for 16 weeks.

Donor Recipient	$ApoE^{-/-}$ $ApoE^{-/-}$ (n=10)	$COMP^{-/-}$ $ApoE^{-/-}$ $ApoE^{-/-}$ (n=14)	$ApoE^{-/-}$ $COMP^{-/-}$ $ApoE^{-/-}$ (n=15)	$COMP^{-/-}$ $ApoE^{-/-}$ $COMP^{-/-}$ $ApoE^{-/-}$ (n=17)
Body weight (g)	32.333±1.202	32.400±0.576	30.105±0.804	33.050±1.540
Blood pressure (mmHg)	108.153±6.876	99.250±3.989	102.498±8.175	107.483±2.571
Plasma COMP (U/L)	9.170±0.962	2.264±0.348 #	5.133±0.578 *#	0.121±0.029#
Complete blood count:				
WBC ($\times10^9$/L)	4.672±0.018	4.894±0.297	4.741±0.168	4.795±0.183
RBC ($\times10^{12}$/L)	8.015±0.817	8.513±0.254	8.180±0.262	8.298±0.360
PLT ($\times10^9$/L)	222.632±26.457	231.198±18.195	245.361±25.815	237.354±14.293
GRN ($\times10^9$/L)	1.298±0.285	1.497±0.104	1.514±0.261	1.384±0.196
LYM ($\times10^9$/L)	1.472±0.163	1.392±0.094	1.528±0.228	1.453±0.069
Serum lipid profile:				
TC (mg/dl)	522.068±88.551	563.342±63.275	504.122±51.416	581.895±61.712
TG (mg/dl)	185.839±55.371	154.862±10.381	163.158±8.590	158.554±15.173
HDL (mg/dl)	32.814±8.810	28.855±5.851	30.258±3.143	32.574±5.198
LDL (mg/dl)	645.159±98.316	519.851±40.480	620.184±57.428	594.291±73.221
Serum biochemical measurements:				
Pi (mM)	1.928±0.096	2.055±0.160	1.858±0.225	1.957±0.165
Ca (mM)	1.803±0.192	1.935±0.241	1.885±0.042	1.858±0.106
BUN (mM)	2.294±0.265	1.787±0.461	2.086±0.254	1.892±0.296
Cre (μM)	26.263±1.725	22.000±3.081	24.752±2.161	23.958±2.057

WBC, white blood cells; **RBC**, red blood cells; **PLT,** platelet; **GRN**, neutrophilic granulocyte; **LYM**, lymphocyte; **TC**, total cholesterol; **TG**, triglycerides; **HDL**, high density lipoprotein; **LDL**, low density lipoprotein; **Pi**, phosphorus; **Ca**, calcium; **BUN**, blood urea nitrogen; **Cre**, creatinine.

Data were presented as Mean±SEM.

***P*<0.05 *vs.* $COMP^{-/-}ApoE^{-/-}$→$ApoE^{-/-}$ chimeric mice.**

***#P*<0.05 *vs.* $ApoE^{-/-}$→$ApoE^{-/-}$ chimeric mice.**

Online Table IV. Body weight, blood pressure and serum lipid profile of ApoE$^{-/-}$ and SMC COMP-Tg mice fed with Western-type diet for 12 weeks.

	ApoE$^{-/-}$ mice (n=11)	SMC COMP-Tg mice (n=10)
Body weight (g)	**34.500±2.019**	**39.269±2.705**
Blood pressure (mmHg)	**100.606±4.764**	**96.583±4.325**
Complete blood count:		
WBC ($\times10^9$/L)	**4.767±0.355**	**4.369±0.287**
RBC ($\times10^{12}$/L)	**8.035±0.526**	**8.425±0.363**
PLT ($\times10^9$/L)	**235.361±25.387**	**228.815±15.944**
GRN ($\times10^9$/L)	**1.205±0.122**	**1.340±0.367**
LYM ($\times10^9$/L)	**1.863±0.325**	**1.504±0.213**
Serum lipid profile:		
TC (mg/dl)	**480.153±38.167**	**465.819±46.185**
TG (mg/dl)	**194.483±14.842**	**188.832±25.093**
HDL (mg/dl)	**28.537±4.967**	**30.054±2.643**
LDL (mg/dl)	**675.632±41.375**	**612.844±29.423**

WBC, white blood cells; **RBC**, red blood cells; **PLT,** platelet; **GRN**, neutrophilic granulocyte; **LYM**, lymphocyte; **TC**, total cholesterol; **TG**, triglycerides; **HDL**, high density lipoprotein; **LDL**, low density lipoprotein.

Data were presented as Mean±SEM.

Online Table V. Correlation analysis of microarrays

Phenotypes	GEO ID	Correlation Factor	*P* Values
M1 (IFN+LPS)	GSE32690	0.05520169	**7.95e-13**
M2a	GSE32690	-0.01034187	0.18
M2b	GSE32690	0.06963045	**< 2.2e-16**
M2c	GSE32690	-0.02911899	**< 0.0001594**
Mox	GSE66782	0.04221708	**8.907e-08**
M1 (LPS)	GSE35436	0.05365392	**3.758e-12**
Osteoclast	GSE46390	-0.0291051	**0.0001659**

Online Table VI. Body weight and serum lipid profile of AAV2-GFP COMP$^{-/-}$ApoE$^{-/-}$ and AAV2-integrin β3 COMP$^{-/-}$ApoE$^{-/-}$ mice fed with Western-type diet for 4 weeks.

	AAV2-GFP COMP$^{-/-}$ApoE$^{-/-}$mice (n=6)	AAV2-integrin β3 COMP$^{-/-}$ApoE$^{-/-}$mice (n=6)
Body weight (g)	**31.465±2.478**	**30.167±2.075**
Serum lipid profile:		
TC (mg/dl)	**475.125±35.683**	**484.468±49.375**
TG (mg/dl)	**183.673±18.392**	**178.033±21.043**
HDL (mg/dl)	**29.865±4.273**	**31.167±2.933**
LDL (mg/dl)	**614.736±36.196**	**598.365±31.687**

TC, total cholesterol; **TG**, triglycerides; **HDL**, high density lipoprotein; **LDL**, low density lipoprotein.

Data were presented as Mean±SEM.

Online Table VII. Body weight and serum lipid profile of AAV2-GFP ApoE$^{-/-}$ and AAV2-β tail domain ApoE$^{-/-}$mice fed with Western-type diet for 4 weeks.

	AAV2-GFP ApoE$^{-/-}$mice (n=8)	AAV2-β tail domain ApoE$^{-/-}$mice (n=6)
Body weight (g)	**29.865±2.537**	**31.033±2.167**
Serum lipid profile:		
TC (mg/dl)	**426.084±31.765**	**445.667±42.143**
TG (mg/dl)	**176.504±21.381**	**184.945±18.284**
HDL (mg/dl)	**30.243±4.323**	**29.439±2.056**
LDL (mg/dl)	**606.753±32.526**	**615.386±30.574**

TC, total cholesterol; **TG**, triglycerides; **HDL**, high density lipoprotein; **LDL**, low density lipoprotein.

Data were presented as Mean±SEM.